Proceedings of the 4th BSME-ASME International Conference on Thermal Engineering
27-29 December, 2008, Dhaka, Bangladesh

UNSTEADY HEAT AND MASS TRANSFER BY MIXED CONVECTION FLOW FROM A VERTICAL POROUS PLATE WITH INDUCED MAGNETIC FIELD, CONSTANT HEAT AND MASS FLUXES

Md. Mahmud Alam, Md. Rafiqul Islam [a] and Fouzia Rahman [a]
Mathematics Discipline, Khulna University, Khulna-9208, Bangladesh
[a] Mathematics Department, Ahsanullah University of Science & Technology, Dhaka, Bangladesh
E-mail: alam_mahmud2000@yahoo.com , mri_sn@yahoo.com

ABSTRACT

Numerical studies are performed to unsteady heat and mass transfer by mixed convection flow from a vertical porous plate with large suction and constant heat & mass fluxes has been studied under the action of transverse applied magnetic field taken into account the induced magnetic field. The boundary layer equations have been transformed into dimensionless coupled nonlinear ordinary differential equations by appropriate transformations. The similarity solutions of the transformed dimensionless equations for the flow field, induced magnetic field, current density, heat and mass transfer characteristics are obtained using shooting iteration technique. Numerical results are presented in the form of velocity, induced magnetic field, and temperature & concentration distributions within the boundary layer for different parameters entering into the analysis. Finally, the effects of the pertinent parameters on the skin-friction coefficient and current density at the plate are also examined.

Keyword: *Induced magnetic field, Heat flux, Mass flux and Mixed convection.*

1. INTRODUCTION

Many transport processes can be found in various ways in both nature and technology, in which the heat and mass transfer by mixed convection flow occur due to the buoyancy force caused by thermal diffusion (temperature difference), mass diffusion (concentration difference). The heat and mass transfer by mixed convection flow has great significance in stellar, planetary, magnetosphere studied and also in the field of aeronautics, chemical engineering and electronics. In many engineering application heat and mass transfer process in fluid condensing or boiling at a solid surface play a decisive role. Boiling and condensing are characteristic for many separation processes in chemical engineering.

Sami and Al-Sanea [1] studied the steady flow and heat transfer characteristics of a continuously moving vertical sheet of extruded material. Chaudhary and Sharma [2] investigated an analytical study of the steady combined heat and mass transfer by mixed convection flow of an incompressible electrically conducting viscous fluid past an electrically non-conducting continuously moving infinite vertical plate with uniform transverse magnetic field, constant heat flux and induced magnetic field. They used perturbation technique to obtain the solution and did not show the complete results due to some analytical restrictions.

Hence our aim is to investigate the steady heat and mass transfer by mixed convection flow from a vertical porous plate with induced magnetic field, thermal diffusion, constant heat and mass fluxes. The governing equations of the problem contain the partial differential equations, which are transformed by similarity transformation into dimensionless ordinary coupled non-linear differential equations and are solved numerically by the sixth order Runge Kutta method along with the Nachtsheim-Swigert iteration technique. The obtained solutions are shown graphically as well as in tabular form.

2. GOVERNING EQUATIONS

Let us consider an unsteady MHD heat and mass transfer by mixed convection flow of an electrically conducting viscous fluid past an infinite vertical porous plate $y = 0$. The flow is also assumed to be in x-direction which is taken along the plate in upward direction and y-axis is normal to it. The temperature and species concentration at the plate are instantly raised from T_w and C_w to T_∞ and C_∞ respectively. Which are thereafter maintained as constant, where T_∞ and C_∞ the temperature and species concentration of the uniform flow respectively. A uniform magnetic field strength **H** is applied to the plate to be acting along the y-axis, which is electrically non-conducting. We assumed that the magnetic Reynolds number of the flow be large enough so that the induced magnetic field is not negligible. The induced magnetic field is of the form $\mathbf{H} = (H_x, H_0, 0)$. The equation of the conservation of electric charge is $\nabla \cdot \mathbf{J} = 0$, where $\mathbf{J} = (J_x, J_y, J_z)$, the direction of propagation is considered only along the y-axis and does not have any variation along the y-axis and the derivative of $\mathbf{J}$ with respect to y namely $\frac{\partial J_y}{\partial y} = 0$, resulting in $J_y =$ constant. Since the plate is electrically non-conducting, this constant is zero and hence $J_y = 0$ every where in the flow. It is assumed that the plate is of infinite extent and the motion is unsteady, so all the physical quantities depend only upon y and t.

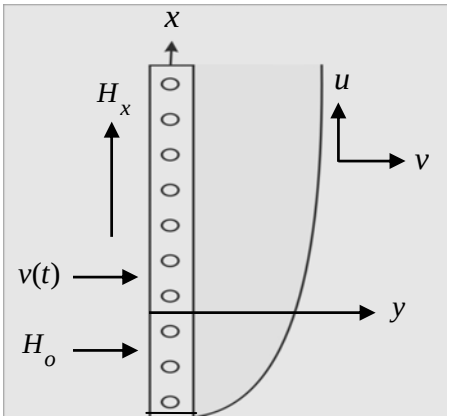

Fig. 1. Physical configuration and coordinate system.

Thus accordance to the above assumptions and Boussinesq approximation, the basic equations relevant to the problem are:

$$\frac{\partial v}{\partial y} = 0 \tag{1}$$

$$\frac{\partial u}{\partial t} + v\frac{\partial u}{\partial y} = g\beta(T - T_\infty) + g\beta^*(C - C_\infty) + \upsilon\frac{\partial^2 u}{\partial y^2} + \frac{\mu_e}{\rho}H_o\frac{\partial H_x}{\partial y} \tag{2}$$

$$\frac{\partial H_x}{\partial t} + v\frac{\partial H_x}{\partial y} = H_o\frac{\partial u}{\partial y} + \frac{1}{\mu_e \sigma'}\frac{\partial^2 H_x}{\partial y^2} \tag{3}$$

$$\frac{\partial T}{\partial t} + v\frac{\partial T}{\partial y} = \frac{k}{\rho c_p}\frac{\partial^2 T}{\partial y^2} + \frac{\upsilon}{c_p}\left(\frac{\partial u}{\partial y}\right)^2 + \frac{1}{\rho c_p \sigma'}\left(\frac{\partial H_x}{\partial y}\right)^2 \tag{4}$$

$$\frac{\partial C}{\partial t} + v\frac{\partial C}{\partial y} = D_m\frac{\partial^2 C}{\partial y^2} + \frac{D_m K_T}{T_m}\frac{\partial^2 T}{\partial y^2} \tag{5}$$

and the boundary conditions for the problem are

$$\left.\begin{array}{llll} t > 0, & u = U_o(t), \quad v = v(t), & \frac{\partial T}{\partial y} = -\frac{q}{k}, \quad \frac{\partial C}{\partial y} = -\frac{m}{D_m}, \quad H_x = H_w & at \quad y = 0 \\ t > 0, & u = 0, & T \to T_\infty, \quad C \to C_\infty, \quad H_x \to 0 & as \quad y \to \infty \end{array}\right\} \tag{6}$$

where all symbols have their usual meaning.

3. MATHEMATICAL FORMULATION

In order to obtain the similarity solutions we introduce a similarity parameter σ as

$$\sigma = \sigma(t) \tag{7}$$

such that σ is the time dependent length scale. In term of this length scale a convenient solution of equation (1) considered to be

$$v(t) = -v_o \frac{\upsilon}{\sigma} \tag{8}$$

where the constant v_o represents a dimensionless normal velocity at the plate, which is positive for suction and negative for blowing.

Now we introduce the following dimensionless variable

$$\eta = \frac{y}{\sigma}, \quad f(\eta) = \frac{u}{U_o}, \ \theta(\eta) = \frac{k}{q\sigma}(T - T_\infty), \quad \phi(\eta) = \frac{D_m}{m\sigma}(C - C_\infty) \quad \text{and} \quad H(\eta) = \frac{\sigma}{\upsilon}\sqrt{\frac{\mu_e}{\rho}}\ H_x$$

Now substituting these equations into the equation (2)-(5), and after simplification we get the following equations in terms of dimensionless variables

$$-[\frac{\sigma}{\upsilon}\frac{\partial\sigma}{\partial t}\eta + v_o]\ f' = f'' + G_r\theta + G_m\phi + MH' \tag{9}$$

$$H'' + P_m[\frac{\sigma}{\upsilon}\frac{\partial\sigma}{\partial t}\eta + v_o]H' + P_m\frac{\sigma}{\upsilon}\frac{\partial\sigma}{\partial t}H + MP_m f' = 0 \tag{10}$$

$$\theta'' + P_r[\frac{\sigma}{\upsilon}\frac{\partial\sigma}{\partial t}\eta + v_o]\theta' - P_r\frac{\sigma}{\upsilon}\frac{\partial\sigma}{\partial t}\theta + E_c P_r(f'^2 + \frac{1}{P_m}H'^2) = 0 \tag{11}$$

$$\phi'' + S_c\left[\frac{\sigma}{\upsilon}\frac{\partial\sigma}{\partial t}\eta + v_o\right]\phi' - S_c\frac{\sigma}{\upsilon}\frac{\partial\sigma}{\partial t}\phi + S_o S_c\theta'' = 0 \tag{12}$$

where $G_r = \frac{q\sigma^3}{\upsilon U_o k}g\beta$ is the Grashof number, $G_m = \frac{m\sigma^3}{\upsilon U_o D_m}g\beta^*$ is the modified Grashof number,

$M = \sqrt{\frac{\mu_e}{\rho}}\frac{H_o}{U_o}$ is the magnetic force number, $P_m = \mu_e\sigma'\upsilon$ is the magnetic diffusivity number,

$P_r = \frac{\rho c_p \upsilon}{k}$ is the Prandtl number, $E_c = \frac{kU_o}{\sigma q c_p}$ is the Eckert number.

$S_c = \frac{\upsilon}{D_m}$ is the Schmidt number and $S_o = \frac{D_m^2 q K_T}{T_m m\upsilon k}$ is the Soret number.

The equations (9)-(12) are similar except the term $\frac{\sigma}{\upsilon}\frac{\partial\sigma}{\partial t}$ where time t appears explicitly. Thus the similarity condition requires that $\frac{\sigma}{\upsilon}\frac{\partial\sigma}{\partial t}$ in equations (9)-(12) must be constant quantity. Hence following the work of Sattar and Alam [3] one can try a class of solutions of the equation (9)-(12) by assuming that

$$\frac{\sigma}{\upsilon}\frac{\partial\sigma}{\partial t} = c \text{ (a constant)} \tag{13}$$

Now from equation (13) we have, $\sigma = \sqrt{2c\upsilon t}$ (14)

It thus appear from (13) that by making a realistic choice of c to be equal to 2 in equation (14), the length scale become equal to $\sigma = 2\sqrt{\upsilon t}$ which exactly corresponds to the usual scaling factor considered for viscous unsteady boundary layer flows (Schlichting, [4]). Since σ is a scaling factor as well as a similarity parameter, any value of c in (14) would not change the nature of solution except that the scale would be different. Finally introducing $c = 2$ in equation (13) we have

$$\frac{\sigma}{\upsilon}\frac{\partial\sigma}{\partial t} = 2 \tag{15}$$

Hence the equation (14)-(17), yields

$$f'' + 2\xi f' + G_r\theta + G_m\phi + MH' = 0 \tag{16}$$

$$H'' + 2\xi P_m H' + 2P_m H + MP_m f' = 0 \tag{17}$$

$$\theta'' + 2\xi P_r \theta' - 2P_r \theta + E_c P_r (f'^2 + \frac{1}{P_m} H'^2) = 0 \tag{18}$$

$$\phi'' + 2\xi S_c \phi' - 2S_c \phi + S_o S_c \theta'' = 0 \tag{19}$$

where $\xi = (\eta + \frac{v_o}{2})$

The corresponding boundary conditions are

$$\left.\begin{array}{l} f = 1, \quad \theta' = -1, \quad \phi' = -1, \quad H = h \text{ (where } h = \dfrac{\sigma}{\upsilon}\sqrt{\dfrac{\mu_e}{\rho}} H_w = 1) \text{ at } \quad \eta = 0 \\ f = 0, \quad \theta \to 0, \quad \phi \to 0, \quad H \to 0 \quad \text{as} \quad \eta \to \infty \end{array}\right\} \tag{20}$$

In all the above equations prime denote the differentiation with respect to η. Hence the equations (16)-(19) give the dimensionless ordinary coupled non-linear differential equations.

4. SKIN FRICTION CO-EFFICIENT AND CURRENT DENSITY AT THE PLATE

The quantities of chief physical interest are the local skin friction coefficient, and the Local Current density at the plate.

The shearing stress at the plate is generally known as the skin friction, the equation defining the local skin friction is

$$\tau = \mu \left(\frac{\partial u}{\partial y}\right)_{y=0} \qquad i.e. \quad \tau \propto f'(0)$$

The current density is generally expressed as $J = -\dfrac{\partial H}{\partial y}$ and hence the current density at the plate is $J_w \propto H'(0)$. The next section deals the solution technique of the problem.

5. NUMERICAL SOLUTION

The set of ordinary coupled non-linear differential equations (16)-(19) with the boundary conditions (20) for unsteady case are very difficult to solve analytically, so numerical procedures are adopted to obtain their solution. Here we use the standard initial value solver, namely the sixth order Runge Kutta method along with Nachtsheim-Swigert iteration technique.

6. RESULTS AND DISCUSSION

To study the physical situation of the problem, we have computed the numerical values of the velocity, induced magnetic field, current density, temperature and concentration within the boundary layer and also the skin friction and current density at the plate for different values of the suction parameter (v_o), the magnetic parameter (M), the Prandtl number (P_r), the Soret number (S_o), the Schmidt number (S_c), the Grashof number (G_r), the magnetic diffusivity parameter (P_m), the Eckert number (E_c) and for the fixed value of modified Grashof number (G_m). The values of G_r is taken to be large (G_r=5.0), since this value corresponds to a cooling problem that is generally encountered in nuclear engineering in connection with the cooling of reactors. The three values 0.71, 1.0 and 7.0 are considered for P_r (in particular, 0.71 represents air at 20^0C, 1.0 corresponds to electrolyte solution such as salt water and 7.0 corresponds to water at 20^0C). The values 0.22, 0.30, 0.60 and 0.78 are also considered for S_c, which represents specific condition of the flow (in particular, 0.22 corresponds to hydrogen, while 0.30 corresponds to helium, 0.60 corresponds to water vapor that represents a diffusivity chemical species of most common interest in air and value 0.78 represents ammonia at temperature 25^0C and 1 atmospheric pressure). The values of v_o, M, S_o, P_m, E_c and G_m are however chosen arbitrarily.

Fig. (2) shows the effect of the suction parameter v_o on the velocity field. This figure depicts that an increase in the suction parameter (v_o) leads to a decrease in the velocity. The usual stabilizing effect of the suction parameter on the boundary layer growth is also evident from this figure. The effect of the magnetic parameter (M) on the velocity field is shown in fig (3). It is observed from this figure that an increase in magnetic parameter (M) leads to an increase in the velocity. Also the stabilizing effect of M on the boundary layer growth is evident It is observed from fig. (4) that the velocity increases within the interval $0 < \eta < 0.42$ (approx.) with the increase of P_m, whereas for roughly after

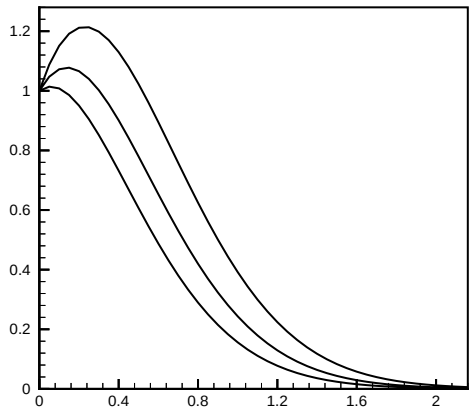

Fig 2. Velocity profiles (f) for different values of v_o, taking G_r=5.0,G_m=2.0, M=1.0, $_m$=1.0, P_r=0.71, S_o=2.0, S_c=0.6 and E_c=0.5 as fixed.

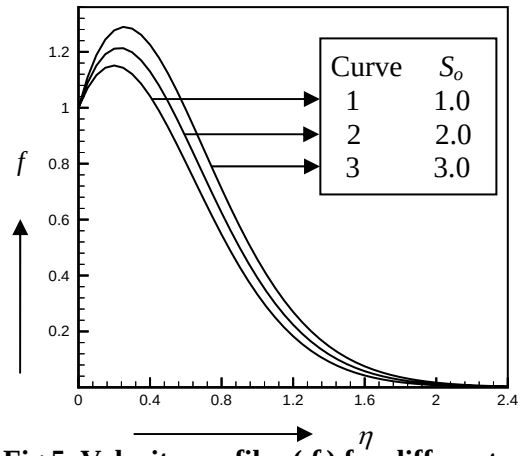

Fig 5. Velocity profiles (f) for different values of S_o, taking v_o =1.0, G_r=5.0, G_m=2.0, M=1.0, P_m=1.0, P_r=0.71, S_c=0.6 and E_c=0.5 as fixed.

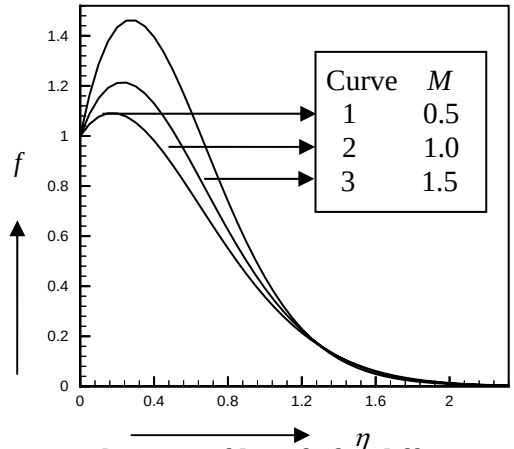

Fig 3. Velocity profiles (f) for different values of M, taking v_o=1.0, G_r=5.0, G_m=2.0, P_m=1.0, P_r=0.71, S_o =2.0, S_c=0.6 and E_c=0.5 as fixed.

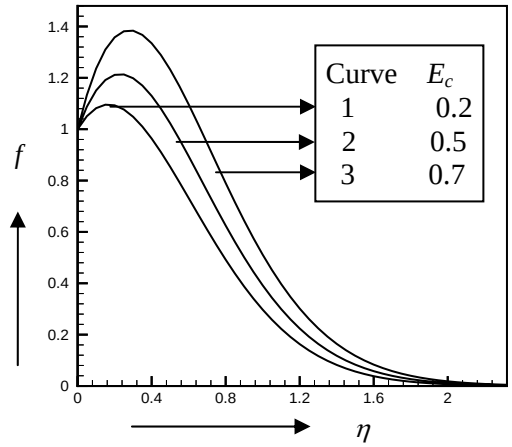

Fig 6. Velocity profiles (f) for different values of E_c , taking v_o=1.0,G_r=5.0, G_m=2.0, M=1.0, P_m=1.0, P_r=0.71, S_0=2.0, and S_c =0.6 as fixed.

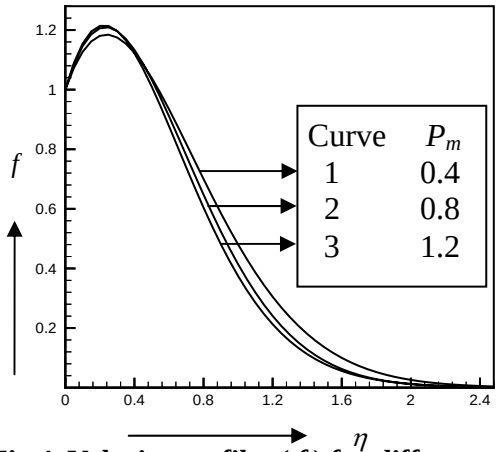

Fig 4. Velocity profiles (f) for different values of P_m, taking v_o =1.0,G_r=5.0, G_m=2.0, M=1.0, P_r=0.71, S_o =2.0, S_c=0.6 and E_c=0.5 as fixed.

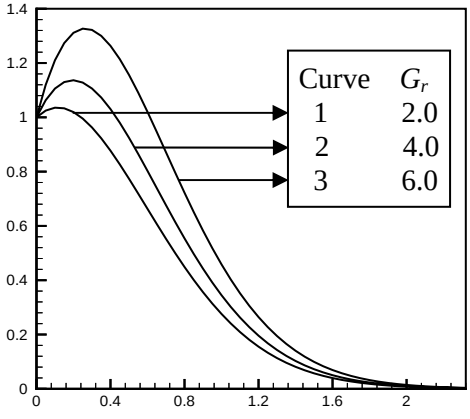

Fig 7. Velocity profiles (f) for different values of G_r , taking v_o =1.0, G_m=2.0, M=1.0, P_m=1.0, P_r=0.71, S_o=2.0, S_c=0.6 and E_c=0.5 as fixed.

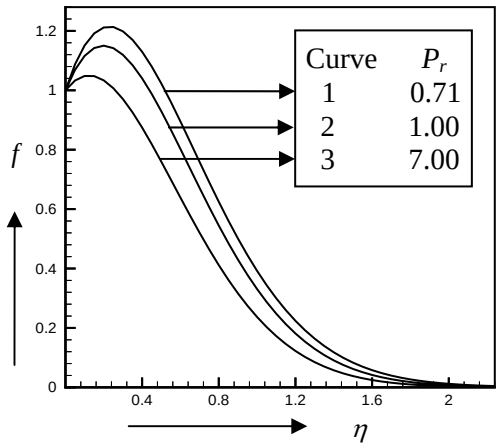

Fig 8. Velocity profiles (f) for different values of P_r , taking v_o =1.0, G_r=5.0, G_m=2.0, M=1.0, P_m=1.0, S_o=2.0, S_c=0.6 and E_c=0.5 as fixed.

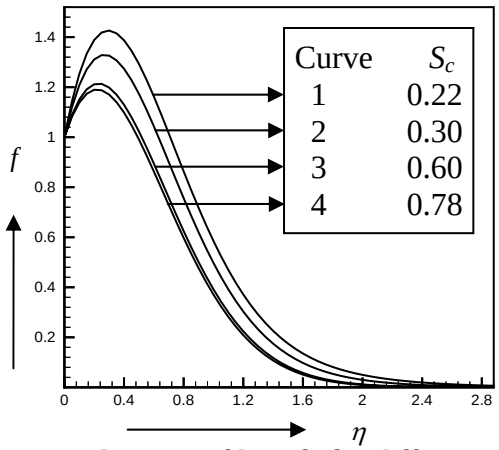

Fig 9. Velocity profiles (f) for different values of S_c , taking v_o=1.0, G_r=5.0, G_m=2.0, M=1.0, P_m=1.0, P_r=0.71, S_o =2.0, and E_c=0.5 as fixed.

$\eta > 0.45$ the velocity decreases with the increase of P_m. In figs.(5), (6) and (7), the variation of the velocity field for different values of Soret number (S_o), Eckert number (E_c) and Grashof number (G_r) are shown respectively. It is observed from these figures that the velocity increases with the increase of S_o, E_c and G_r. In figs (8) and (9), the variation of the velocity field for different values of P_r and S_c are shown respectively. From these figures, it is seen that the velocity decreases with the increase of P_r and S_c. It is seen from figs.(2)-(9), the effect of the various parameters on the velocity profiles is more prominent when $\eta = 0.3$ (approximately).It is also seen from fig. (9) that the velocity is more for hydrogen (S_c =0.22 at temperature 25^0C and 1 atmospheric pressure) than ammonia (S_c=0.78 at temperature 25^0C and 1 atmospheric pressure).

7. CONCLUSION

The usual stabilizing effect of the suction parameter on the boundary layer growth is also evident. Both the velocity and the temperature profiles increase with the increase of M, S_o, E_c and G_r. Also both the velocity and concentration profiles increase with the increase of the Sorret number (S_o). The species concentration is an exponentially decreasing function of y. The maximum concentration occurs near the plate and it tends to zero as y tends to infinity.

8. REFERENCES

[1] Sami, A. and Al-Sanea, International Journal of Heat Mass Transfer, 47, (2004), pp. 14-45.
[2] Chaudhary, R.C. and Sharma, B. K., Journal of Applied Physics, 99 (2006), pp. 034901.
[3] Sattar and Alam, Indian J.Pure Applied Math., 25, (1994), 6, pp. 679-688.
[4] Schlichting, H., Boundary Layer Theory, McGraw-Hill, New York, (1968).

Proceedings of the 4th BSME-ASME International Conference on Thermal Engineering
27-29 December, 2008, Dhaka, Bangladesh

NATURAL CONVECTION FLOW ALONG THE WAVY CONE IN CASE OF UNIFORM SURFACE HEAT FLUX WITH TEMPERATURE DEPENDENT VISCOSITY

A. Rahman[1], M. M. A. Sarker[2], N.E. Mustafa[1], M. M. Molla[3]

[1]Department of Natural Science, Stamford University Bangladesh, Dhaka, Bangladesh
[2]Department of Mathematics, Bangladesh University of Engineering & Technology, Dhaka, Bangladesh
[3]Department of Mechanical Engineering, University of Glasgow, Glasgow G12 8QQ, UK
(azadrahman@gmail.com)

ABSTRACT

The effect of temperature dependent viscosity μ(T), on steady two dimensional natural convection flow along a vertical wavy cone with uniform surface heat flux has been investigated. Viscosity is considered to be a linear function of temperature. Using the appropriate variables, basic equations are transformed to non-dimensional boundary layer equations and then solved numerically employing implicit SFFD method. The effects of viscosity variation parameter on the velocity profile, temperature profile, skin friction, average Nusselt number and isotherm have been discussed.

Key words: *Natural convection, wavy cone, viscosity variation parameter, heat flux.*

1. INTRODUCTION

Wavy surfaces are encountered in several heat transfer devices such as flat plate solar collectors and flat plate condensers in refrigerators. Larger scale surface non-uniformities are encountered in cavity wall insulating systems and grain storage containers etc. If the surface is wavy, the flow is disturbed by the surface and this alters the rate of heat transfer.

The papers to date that study the effects of such non-uniformities on the vertical convective boundary layer flow of a Newtonian fluid are those of Yao [1], Moulic and Yao [2, 3]. Natural convection over a vertical wavy cone and frustum of a cone has been studied by Pop and Na [4, 5]. Hossain et al. [6, 7, 8] have studied the problem of natural convection flow along a vertical wavy cone and wavy surface with uniform surface temperature in presence of temperature dependent viscosity. In all of the above mentioned studies except Hossain et al. [6, 7, 8], the authors considered that the viscosity of the fluids are constant in the flow regime. But the physical properties may change significantly with temperature. For instance, the viscosity of water decreases about 240% when the temperature increases from 10^{o}C to 50^{o}C. Chrraudeau [9] have considered the viscosity of the fluid to be proportional to a linear function of temperature. Very few of the aforementioned authors have studied natural convection flow for a surface which exhibits the uniform surface heat flux.

In the present study, the natural convection boundary layer flow along a vertical wavy cone with uniform heat flux has been considered. In addition, the viscosity of the fluid is taken to be a linear function of the temperature. The current problem is solved numerically by using Straightforward Finite Difference method (SFFD), reported by Yao [1, 2]. Solutions are obtained for the fluid having Prandtl number Pr = 0.7 (air) and with the different values of viscosity variation parameter.

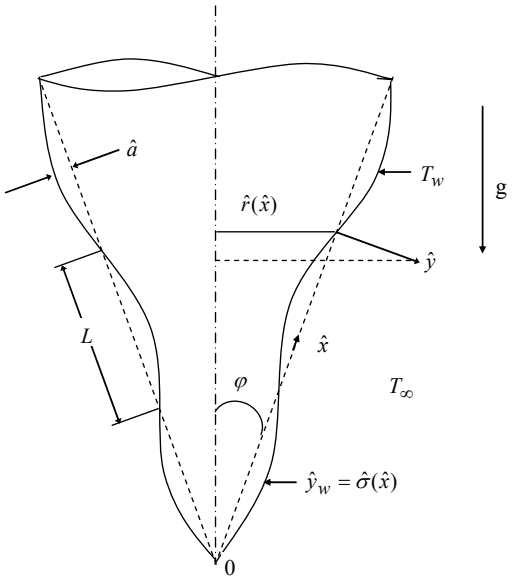

Fig. 1: Physical model and the coordinate system

2. FORMULATION OF THE PROBLEM

The boundary layer analysis outlined below allows the shape of the wavy surface, $\hat{\sigma}(\hat{x})$ to be arbitrary, but our detailed numerical work will assume that the surface exhibits sinusoidal deformations. Thus the wavy surface of the cone is given by

$$\hat{y}_w = \sigma(\hat{x}) = \hat{a}\sin(\pi\,\hat{x}/L) \tag{1}$$

Where L is the half of the fundamental wave length and $\hat{a}$ is the amplitude of the wavy cone. The physical model of the problem and the two-dimensional coordinate system are shown in fig.1, where $\hat{r}(\hat{x})$ the local radius of the flat surface of the cone is defined by

$$\hat{r} = \hat{x}\sin\varphi \tag{2}$$

Under the Boussinesq approximation, we consider the flow to be governed by the following equations:

$$\frac{\partial(\hat{r}\,\hat{u})}{\partial\hat{x}} + \frac{\partial(\hat{r}\,\hat{v})}{\partial\hat{y}} = 0 \tag{3}$$

$$\hat{u}\frac{\partial\hat{u}}{\partial\hat{x}} + \hat{v}\frac{\partial\hat{u}}{\partial\hat{y}} = -\frac{1}{\rho}\frac{\partial\hat{p}}{\partial\hat{x}} + \frac{1}{\rho}\overline{\nabla}.(\mu\overline{\nabla}\hat{u}) + g\beta(T - T_\infty)\cos\varphi \tag{4}$$

$$\hat{u}\frac{\partial\hat{v}}{\partial\hat{x}} + \hat{v}\frac{\partial\hat{v}}{\partial\hat{y}} = -\frac{1}{\rho}\frac{\partial\hat{p}}{\partial\hat{y}} + \frac{1}{\rho}\overline{\nabla}.(\mu\overline{\nabla}\hat{v}) + g\beta(T - T_\infty)\sin\varphi \tag{5}$$

$$\hat{u}\frac{\partial T}{\partial\hat{x}} + \hat{v}\frac{\partial T}{\partial\hat{y}} = \frac{k}{\rho C_p}\overline{\nabla}^2 T \tag{6}$$

where $(\hat{x},\hat{y})$ are the dimensional coordinates and $(\hat{u},\hat{v})$ are the velocity components parallel to $(\hat{x},\hat{y})$. Here $\hat{p}$ is the pressure of the fluid and *Cp* is the specific heat at constant pressure. Here μ is the temperature dependent viscosity of the fluid, given by

$$\mu = \mu_\infty[1 + \gamma(T - T_\infty)] \tag{7}$$

The boundary condition for the present problem is

$$\hat{u} = 0,\ \hat{v} = 0,\ \ q_w = -k(\hat{n}.\overline{\nabla}\hat{T}) \text{ at } \hat{y} = \hat{y}_w = \sigma(\hat{x}) \tag{8a}$$

$$\hat{u}=0, \quad T=T_\infty \text{ as } \hat{y}\to\infty \tag{8b}$$

Now the following non-dimensional variables are introduced to obtain a set of non-dimensional governing equation:

$$x=\frac{\hat{x}}{L}, \quad y=\frac{\hat{y}-\sigma(\hat{x})}{L}Gr^{1/5}, \quad r=\frac{\hat{r}}{L}, \quad a=\frac{\hat{a}}{L}, \sigma(x)=\frac{\sigma(\hat{x})}{L}, \quad \sigma_x=\frac{d\hat{\sigma}}{d\hat{x}}=\frac{d\sigma}{dx},$$

$$p=\frac{L^2}{\rho\nu_\infty{}^2}Gr^{-4/5}\hat{p}, \quad u=\frac{\rho L}{\mu_\infty}Gr^{-2/5}\hat{u}, \quad v=\frac{\rho L}{\mu_\infty}Gr^{-1/5}\left(\hat{v}-\sigma_x\hat{u}\right),$$

$$\theta=\frac{T-T_\infty}{(q_wL/k)}Gr^{1/5}, \quad Gr=\frac{g\beta q_w\cos\varphi}{k\nu_\infty{}^2}L^4, \ \mathrm{Pr}=\mu_\infty C_p/k, \ \varepsilon=(q_wL/k)\gamma Gr^{-1/5} \tag{9}$$

Here the new coordinate system (x, y) are not orthogonal, but a regular rectangular computational grid can be easily fitted in the transformed coordinate. After transforming the governing equations the term $\partial p/\partial y$ is eliminated from the momentum equations to obtain a combined momentum equation of the following form

$$u\frac{\partial u}{\partial x}+v\frac{\partial u}{\partial y}=(1+\varepsilon\theta)\left(1+\sigma_x{}^2\right)\frac{\partial^2 u}{\partial y^2}+\varepsilon\left(1+\sigma_x{}^2\right)\frac{\partial\theta}{\partial y}\frac{\partial u}{\partial y}-\frac{\sigma_x\sigma_{xx}}{1+\sigma_x{}^2}u^2+\frac{(1+\sigma_x\tan\varphi)}{1+\sigma_x{}^2}\theta \tag{10}$$

More details about the transformation can be found on Rahman. A. [10]

3. NUMERICAL METHODS

To investigating the present problem, the straightforward finite difference method (SFFD) is applied, which is described below. Firstly we introduce the following transformations to reduce the governing equation to a convenient form:

$$\begin{aligned} &X=x, \quad Y=y/(5x)^{1/5}, \quad R=r, \quad U(X,Y)=u/(5x)^{3/5}, \\ &V(X,Y)=(5x)^{1/5}v, \quad \Theta(X,Y)=\theta/(5x)^{1/5} \end{aligned} \tag{11}$$

Introducing the transformations into the governing equation we obtain the following form,

$$8U+(5X)\frac{\partial U}{\partial X}-Y\frac{\partial U}{\partial Y}+\frac{\partial V}{\partial Y}=0 \tag{12}$$

$$\begin{aligned} (5X)U\frac{\partial U}{\partial X}+(V-YU)\frac{\partial U}{\partial Y}+\left\{3+\frac{\sigma_x\sigma_{xx}}{1+\sigma_x{}^2}(5X)\right\}U^2 &=\left\{1+\varepsilon\ (5X)^{1/5}\Theta\right\}\left(1+\sigma_x{}^2\right)\frac{\partial^2 U}{\partial Y^2} \\ &+(5X)^{1/5}\varepsilon\left(1+\sigma_x{}^2\right)\frac{\partial\Theta}{\partial Y}\frac{\partial U}{\partial Y}+\frac{(1+\sigma_x\tan\varphi)}{1+\sigma_x{}^2}(5X)^{1/5}\Theta \end{aligned} \tag{13}$$

$$(5X)U\frac{\partial\Theta}{\partial X}+(V-YU)\frac{\partial\Theta}{\partial Y}+U\Theta=\frac{1}{\mathrm{Pr}}\left(1+\sigma_x{}^2\right)\frac{\partial^2\Theta}{\partial Y^2} \tag{14}$$

The boundary conditions of the problem take the final form:

$$\begin{aligned} &U=0, \quad V=0, \quad \frac{\partial\Theta}{\partial Y}=-1/\sqrt{1+\sigma_x^2} \text{ at } Y=0 \\ &U=0, \quad \Theta=0 \text{ as } Y\to\infty \end{aligned} \tag{15}$$

Solutions of the non-dimensional partial differential system given by (12)-(14) and subject to the boundary conditions (15) are obtained by using the straightforward finite difference method reported by L.S. Yao [1, 2].

However, once we know the values of the function U, V and Θ along with their derivatives, it is important to calculate the values of the average Nusselt number, Nu_m from the following relation which is obtained by using the set of transformations:

$$Nu_m (5/Gr)^{1/5} = \frac{X^{1/5}\int_0^X \sqrt{1+\sigma_x^2}\, dX}{\int_0^X \sqrt{1+\sigma_x^2}\cdot X^{1/5}\cdot \Theta(X,0)\, dX} \tag{16}$$

The skin friction coefficients is defined as

$$C_{f_x} (Gr)^{1/5} \Big/ \{2(5X)^{2/5}\} = \left(1+\varepsilon\,(5X)^{1/5}\Theta\right)\sqrt{1+\sigma_x^2}\,\frac{\partial U}{\partial Y}\Big]_{Y=0} \tag{17}$$

4. RESULTS AND DISCUSSION

In this paper, the effect of temperature dependent viscosity on a steady two-dimensional natural convection laminar flow of viscous incompressible fluid along a vertical wavy cone has been investigated by using very efficient finite difference method. It is seen that the solutions are affected by the viscosity variation parameter, ε. So we focus our attention on the effect of ε on the average Nusselt number $\mathrm{Nu_m}(5/\mathrm{Gr})^{1/5}$, skin friction $C_{fx}(Gr)^{1/5}/\{2(5x)^{2/5}\}$ as well as velocity and temperature distribution. We also show the graphical representation of isotherms pattern of the flow field. In each case a = 0.3 and φ = 30^o are considered for the numerical solutions.

At first it should be mentioned that without viscosity variation parameter (i.e. for ε = 0.0) and for the case of a flat cone (i.e. a = 0), we recover the problem discussed by Lin [11]. Fig. 2(a)-(c) represents the non-dimensional tangential, normal velocity distribution and temperature distribution for different values of ε at a fixed point X = 1.0. From the tangential velocity distribution it is clear that the increasing value of ε decrease the tangential velocity inside the boundary layer. As viscosity is a linear function of temperature, increasing value of ε indicate rapid change of viscosity towards upstream, which causes the decrease of fluid velocity. Fig. 2(b) shows that the normal velocity enhances when ε increases but decreases for the increases of Y values. From the fig. 2(c) it is evident that the temperature inside the boundary layer at any fixed point increases when ε increases.

The effects of ε on the surface temperature, skin friction coefficient and on the average Nusselt number are given in the fig. 3(a)-(c) respectively. It was found that the wall temperature increases significantly due to the increasing value of ε. Also skin friction increases throughout the computational domain with increases of ε. As ε increases, the viscosity increases with temperature which results the increase of skin friction. Also we have found that the amplitude of the skin friction distribution enhanced with ε, while the average rate of heat transfer decreases when ε increases.

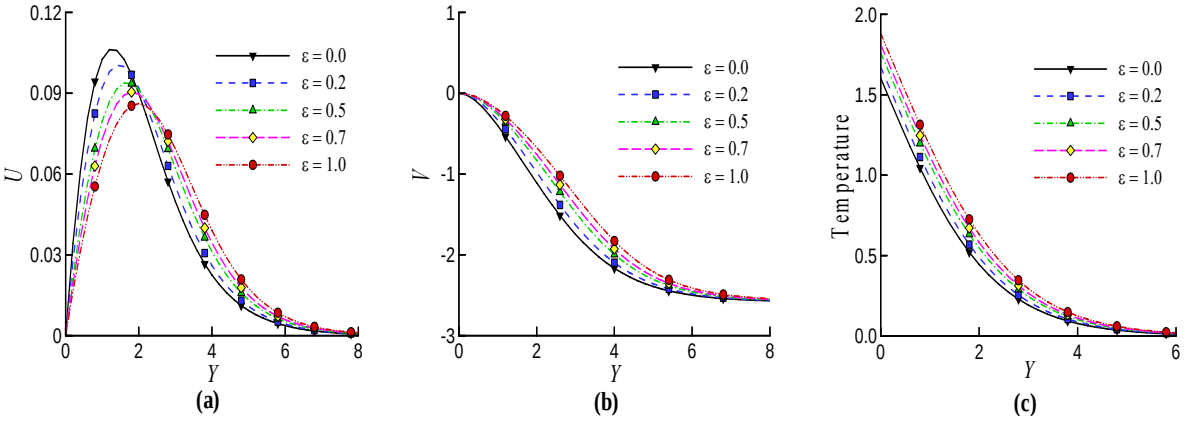

Fig. 2: (a) Tangential velocity distribution and (b) Normal velocity distribution and (c) Temperature distribution at X =1.0

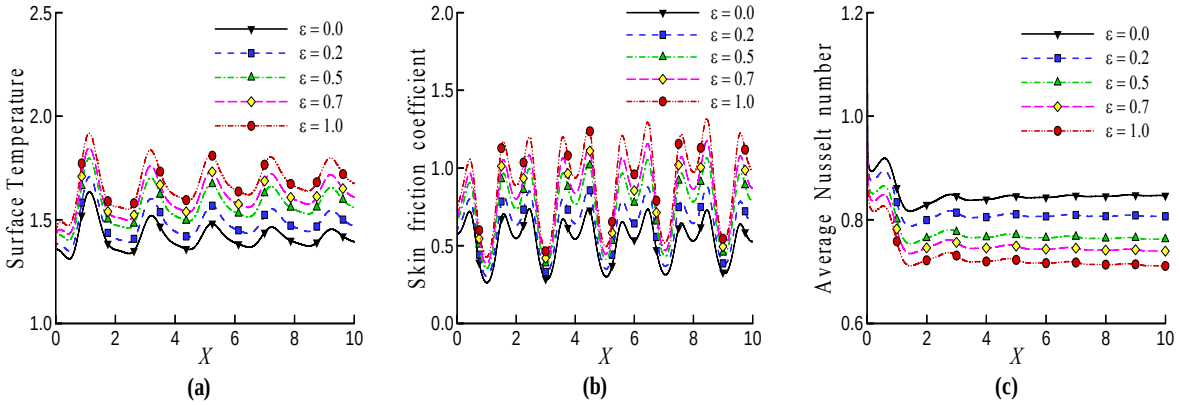

Fig. 3: (a) Surface temperature (b) Skin friction coefficient and (c) Average Nusselt number for different ε

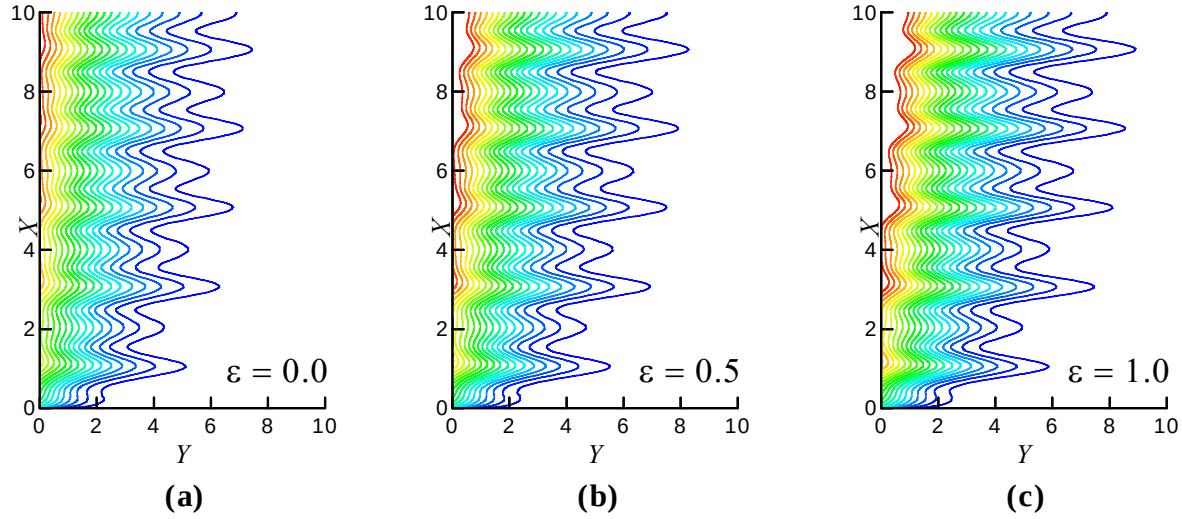

Fig. 4: Isotherms for different values of viscosity variation parameter ε

Fig. 4(a)-(c) show the isotherm for a wavy cone with $a = 0.3$, $\varphi = 30^{o}$, while the viscosity variation parameter ε are taken as 0.0, 0.5 and 1.0 respectively. The figures indicate that with the increase of ε, the thickness of thermal boundary layer increases slightly.

5. CONCLUSIONS

The effect of viscosity variation parameter ε, on the natural convection boundary layer flow along a vertical wavy surface with uniform heat flux, has been studied numerically using very efficient straightforward finite difference (SFFD) method. The result can be summarized as follows:

- The skin friction increases with the increase of viscosity variation parameter ε.
- The average Nusselt number decreases significantly for increasing value of viscosity.
- Tangential velocity reduces with the increasing value of viscosity variation parameter.
- Fluid temperature and surface temperature were found to increase with the increases of ε.
- For the increases of ε, the thickness of thermal boundary layer increases slightly.
- Ignoring the viscous effect may introduce sever error while predicting surface rate of heat transfer and skin friction coefficient.

NOMENCLATURE

a	Amplitude wavelength ratio
C_f	Skin friction coefficient
Gr	Grashof number
k	Thermal conductivity [$Wm^{-1}K^{-1}$]
$\hat{n}$	Unit vector normal to the surface
Nu_m	Average Nusselt number
p	Dimensionless pressure function
Pr	Prandtl number
q_w	Uniform heat flux [Wm^{-2}]
$\hat{r}(\hat{x})$	Local radius of the of the cone [m]
r, R	Dimensionless radius of the cone
T	Temperature on boundary layer [K]
T_∞	Temperature of ambient fluid [K]
T_w	Temperature at the surface [K]
(u, v)	Dimensionless velocity component
Greek symbols	
β	Volumetric coefficient of thermal expansion [K^{-1}]
ε	Viscosity variation parameter
θ, Θ	Dimensionless temperature function
μ	Viscosity of the fluid [$kg.m^{-1}s^{-1}$]
μ_∞	Dynamic viscosity of the ambient fluid [$kg.m^{-1}s^{-1}$]
ν_∞	Reference kinematic viscosity [m^2s^{-1}]
ρ	Density of the fluid [$kg\ m^{-3}$]
$\sigma(x)$	Non-dimensional surface profile
τ_w	Shearing stress [$kg\ m^{-1}s^{-2}$]
φ	The half angle of the cone
ψ	Stream function [m^2s^{-1}]
Subscript	
m	Average condition
∞	Ambient condition
x	Differentiation with respect to x

REFERENCES

[1] Yao, L. S., Natural convection along a vertical wavy surface, ASME J. Heat Transfer vol. 105 (1983), pp. 465–468.

[2] Moulic, S. G. and Yao, L. S., Natural convection along a wavy surface with uniform heat flux, ASME J. Heat Transfer vol.111 (1989), pp.1106–1108.

[3] Moulic, S. G. and Yao, L. S., Mixed convection along wavy surface, ASME J. Heat Transfer vol. 111 (1989), pp. 974–979.

[4] Pop, I. and Na, T. Y., Natural convection from a wavy cone, applied Scin. Res. vol. 54 (1995), pp. 125–136.

[5] Pop, I. and Na, T. Y., Natural convection over a vertical wavy frustum of a cone, Int. J. Non-Linear Mech. vol. 34 (1999), pp. 925–934.

[6] Hossain, M. A., Munir, M. S. and Pop, I., Natural convection flow of viscous fluid with viscosity inversely proportional to linear function of temperature from a vertical cone, Int. J. Therm. Sci. vol. 40 (2001), pp. 366–371.

[7] Hossain, M. A., Munir, M. S. and Pop, I., Natural convection of a viscous fluid with variable viscosity and thermal conductivity from a vertical wavy cone, Int. J. Therm. Sci., vol. 40 (2001), pp. 437–443.

[8] Hossain, M. A., Kabir, S. and Rees, D. A. S., Natural convection of fluid with temperature dependent viscosity from heated vertical wavy surface, ZAMP 53 (2002), pp. 48–52.

[9] Chrraudeau, J., Influence de gradients de proprietes physiques en convection force application au cas du tube, Int. J. Heat Mass Tran. vol. 18 (1975), pp 87–95.

[10] Rahman, A., Natural convection flow over the wavy cone with temperature dependent viscosity in case of surface heat flux, M.Phil. Thesis, Dept. of Mathematics, BUET, 2008.

[11] Lin, F. N., Laminar convection from a vertical cone with uniform surface heat flux, Letters in Heat and Mass Transfer, vol. 3 (1976), pp. 49-58.

Proceedings of the 4th BSME-ASME International Conference on Thermal Engineering
27-29 December, 2008, Dhaka, Bangladesh.

CONTROL OF WATER HEAT RECOVERY CHILLER USING SPLIT CONDENSER HEAT RECOVERY CHILLER SYSTEM

Md. Iqbal Mahmud[1], Haeng Muk Cho[2] and M. Iqbal[3]

[1, 2] Division of Mechanical and Automotive Engineering, Kongju National University,
275 Boodae-dong, Cheonan, Chungnam 330-717, South Korea.

[3]Department of Industrial and Production Engineering,
Shahjalal University of Science and Technology (SUST), Sylhet-3114, Bangladesh.
Email: mimchanchal@yahoo.com

ABSTRACT

By using the heat recovery of water-cooled chillers, it is possible to reduce the energy operating costs positively and at the same time it could fulfill the heating re-heat air conditioning system as well as the hot water requirements. Design of higher water temperature requirements and split condenser heat recovery chiller system (using of templifiers) produced hotter condenser water up to 140°F (60°C) and control the entire heat recovery system.

KEYWORDS: *Heat Recovery Chillers, Split Condenser, Templifier.*

1. INTRODUCTION

Through cooling towers, water-cooled chiller discharges a significant amount of heat. In this manner all of the building heat and the heat generated by the compressor work leave the building. Reclaiming this heat and using in to heat the building or the domestic hot water can potentially offer huge energy savings. The water temperature must be increased for improving the value of the rejected heat. When there is a source (a cooling load in the building) and a requirement (a heating load in the building) then the heat recovery occurs. The viability of condenser heat recovery can dictates by different Heating, Ventilation and Air Conditioning (HVAC) system types and building uses. From the condenser heat recovery, high domestic hot water usage such as health care, hotels etc can also be benefited.

2. HEAT RECOVERY METHODS

Generally two kinds of heat recovery methods are widely used. One is using a heat exchanger and another is using additional condenser.

According to the figure-1, outside of the water-cooled condenser one heat exchanger is used. The set up shows instead of rejecting the heat to the cooling tower (finally goes to the environment); heat is recovered from the condenser water and the heating water temperature is lower due to an additional heating transfer heat exchanger.

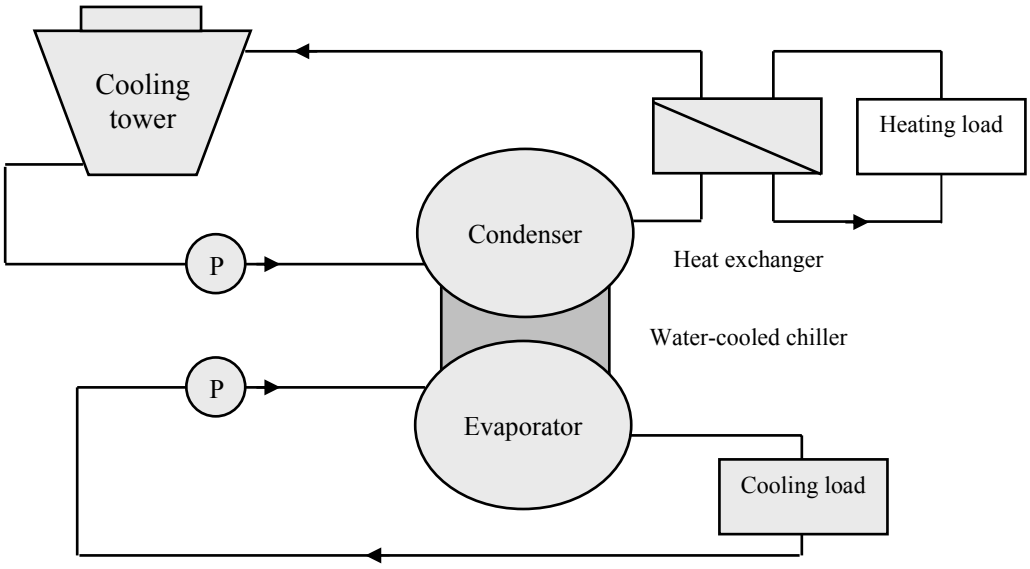

Figure-1: Heat recovery using heat exchanger

According to the figure-2, by using an additional condenser bundle (piped in parallel with the standard condenser) the heat recovery could take place directly from hot refrigerant in the refrigeration circuit. Here the cooling tower circuit and the heating circuit are separate. As there is no heat exchanger, the heating water temperature is higher due to direct heat transfer by the heat recovery condenser.

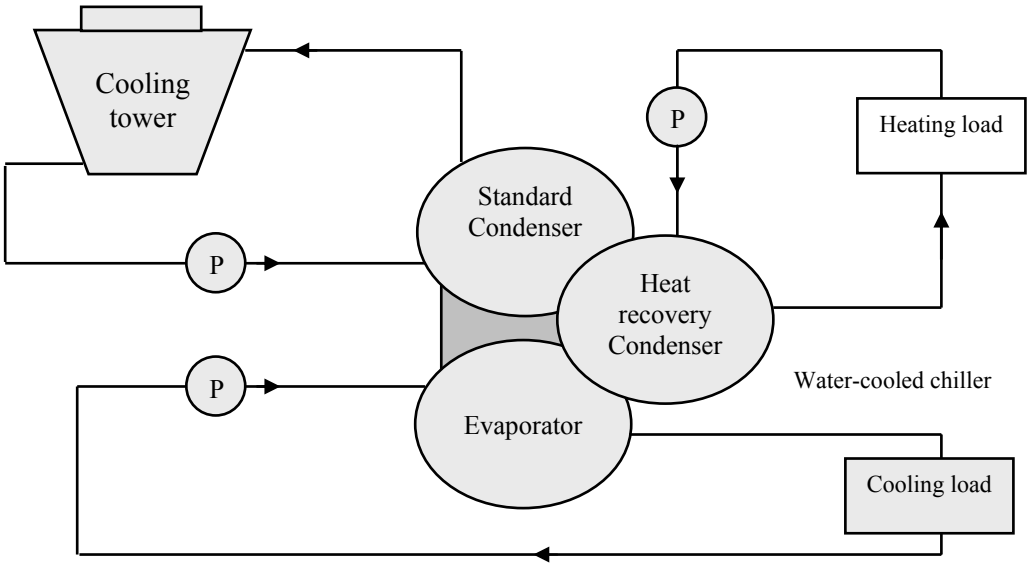

Figure-2: Heat recovery using an additional condenser

3. MAJOR CONCERNS OF HEAT RECOVERY

3.1 Maximum amount of heat recovery

Theoretically, the heat amount is equal to the summation of cooling load and compressor power. By using an additional heat recovery condenser, maximum amount of heat recovery could be up to 100% of cooling capacity for centrifugal water chillers.

3.2 The highest heating water temperature

Figure 1 and figure 2 shows, from the cooling load the heat recovery chiller removes heat in the evaporator to the condenser. Then it recovers heat rejection from the condenser to the cooling tower. For making it cooling, heat cannot be recovered without cooling. Here the higher heating water temperature is the lower efficiency and cooling capacity. Heating water at 109.4ºF to 118.4ºF (43ºC to 48ºC) is available for heat recovery centrifugal chillers. Therefore, an auxiliary heat source is needed for higher heating water temperature requirements.

3.3 Heating water temperature and control

Generally, for designing heating water temperature, for every 42.08ºF (5.6ºC) temperature increases heat recovery power consumption increases from 7% to 14%. In most cases, the heating water temperature control designs to maintain the return heating water temperature. Allowing the supply heating water temperature to in the system drops as the chiller load decreases and less heat is rejected to the condenser (figure-3). Though the mean water temperature drops the refrigerant condensing temperature and pressure difference at which the compressor is required to produce at part load.

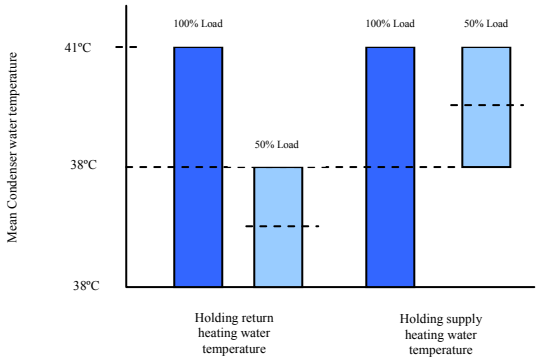

Figure-3: Heating water control temperature

4. FEATURES OF HEAT RECOVERY CHILLERS

Heat recovery chillers basically produced higher leaving condenser water temperature. Therefore, it does not duplicate the energy efficiencies of cooling only machines. Figure-4 shows, the typical operating cycles of a cooling only machine and a heat recovery machine. The main differences between the two machines are:

(a) The pressure difference (provided by the compressor) is much greater for heat recovery cycle than the cooling cycle.

(b) The amount of heat rejected from the heat recovery condenser is greater than the heat rejected from the cooling only operation.

(c) The heat recovery machine has lower energy efficiency during heat recovery operations.

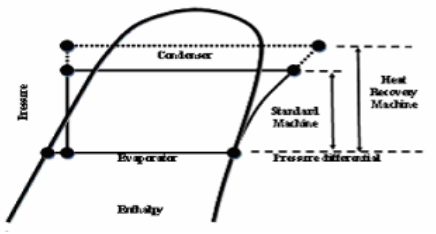

Figure-4: Refrigerant pressure difference

5. HEAT RECOVERY OPERATION USING SPLIT CONDENSERS

Split condenser chiller is most common and widely used system for heat recovery operations. Figure-5 shows a split condenser heat recovery chiller system, which does not require a heat exchanger. As the chillers produced hotter condenser water, it work harder and its performance drops when compared to conventional chilled water production. This loss must be weighted against the value of producing usable hot temperature water. Maximum heating systems are designed to operate at 180ºF (82.22ºC) supply water. During heat recovery mode, the heating system must be able to meet the requirements of the building with only 105ºF to 110ºF (40.55ºC to 43.33ºC) water. This may require changes to the heating system design that will increase capital cost as well as operating cost.

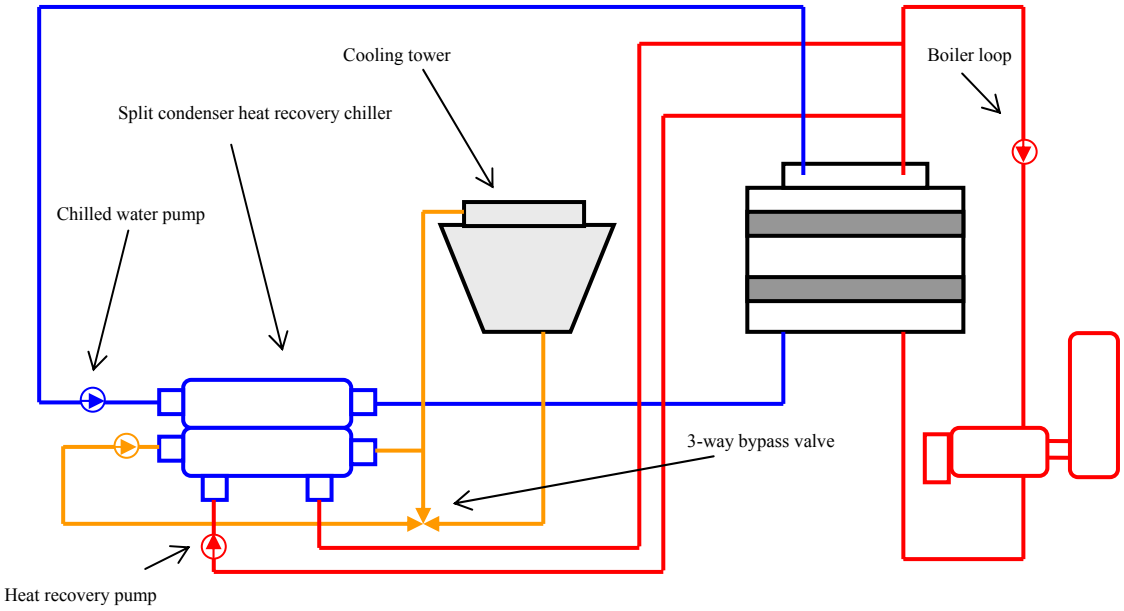

Figure-5: Split condenser heat recovery chillers

Secondly, several heat pumps (known as templifiers), which recover low-grade heat and convert the low-grade heat into high-grade heat. In the condenser water application it produces 140ºF to 160ºF (60ºC to 71.11ºC) hot water from condenser water heat. Higher water temperature produce by the templifiers reduces the impact on the entire heating system

but it has a minimal impact on the chilled water plant operation. The templifier can produce enough hot water to directly heat the storage tank.

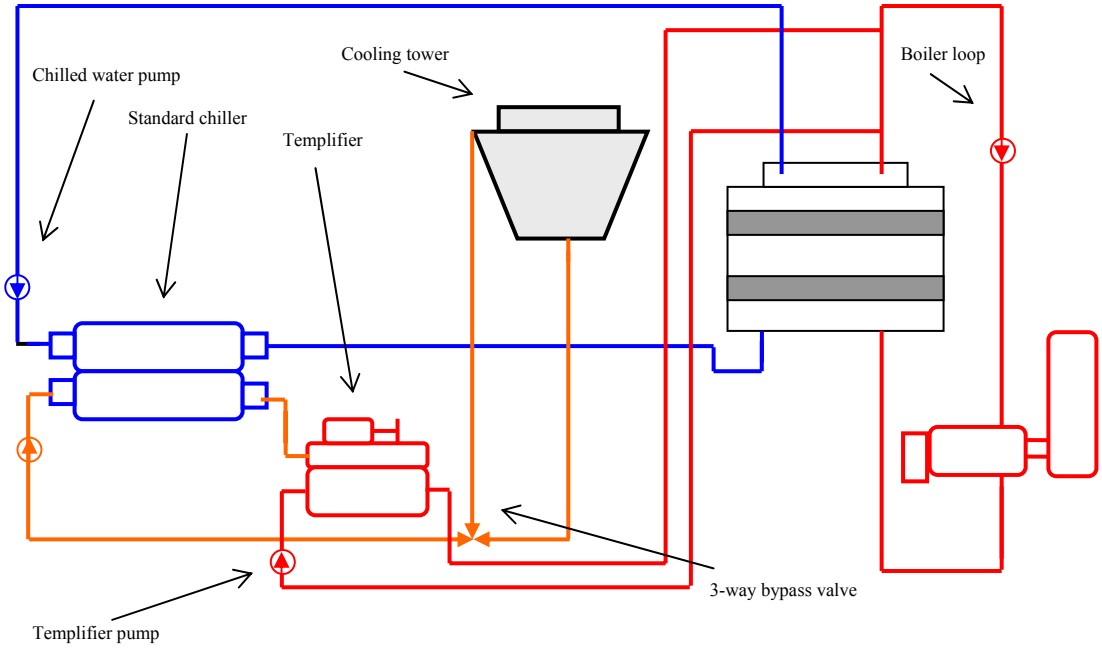

Figure-6: Templifier application in split condenser heat recovery chillers

The system has the following advantages:

(a) The system can recover large amount of heat that somehow rejected from the building and then use it for other purposes such as building heat or domestic hot water heating.

(b) The system can be used with any kind of water-cooled chiller plant and any HVAC system that has simultaneous heating and cooling requirements.

(c) Heat recovery chillers are only preheat the domestic hot water make up but using of templifier causes heat of domestic hot water up to 140ºF (60ºC) even if there is no flow in to the storage tank.

6. DESIGN FOR HIGHER WATER TEMPERATURE

Figure-7 shows, two chillers overlap in series which recovering cooling load heat rejection from the first stage chillers condenser water on the way to the cooling tower. Then delivering the heat to the heat load by the second stage chiller in series for higher heating from water temperature up to 140ºF (60ºC). Heat removed from the cooling then delivered to the heating load through the following water circuit loop, cooling tower, the first stage chillers condenser, the second stage chillers evaporator, cooling tower. If the heating load could not match the cooling load, the cooling tower rejects any leftover heat to the atmosphere.

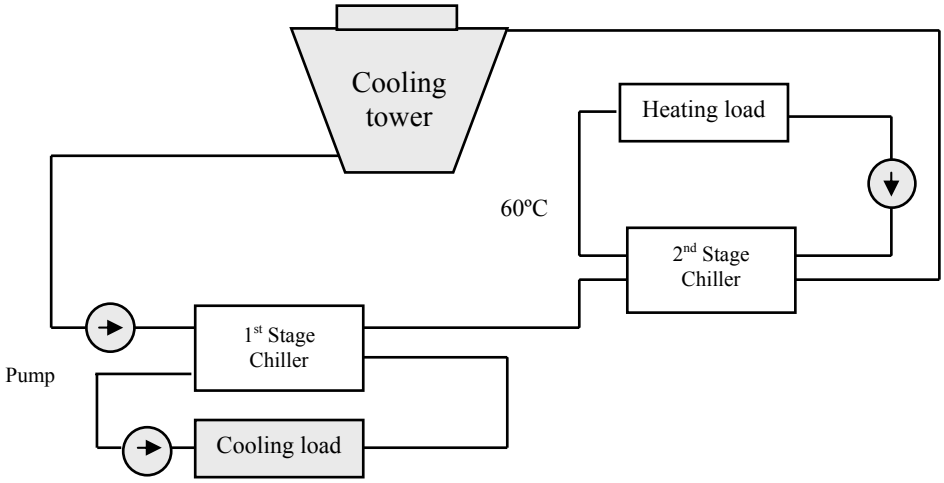

Figure-7: Design for higher water temperature

7. CONCLUSIONS

Water heat recovery through condenser could be used whenever there are simultaneous heating and cooling loads. Heating load could be either for domestic hot water or building heating. Using split condensers in the heat recovery system produces higher temperature water and the heat recovery chillers can provide more heat with less efficiency than operating in cooling only mode. Therefore, the major concerns of heat recovery system and the two chillers overlap in series can control the water heat recovery and higher water temperature.

8. REFERENCES

[1] J. Jing, Introduction of heat recovery chiller control and water system design.
[2] Khurmi R. S. and Gupta J. K., "A Text book of Thermal Engineering", (2004).
[3] EarthWise CenTraVac Water-cooled Liquid Chillers, Trane literature, CTV- PRC007-EN.
[4] Heat Recovery Centrifugal Chillers and Templifier Water Heaters, McQuary Brochure, A/SP HR (01/03)

Proceedings of the 4th BSME-ASME International Conference on Thermal Engineering
27-29 December, 2008, Dhaka, Bangladesh

VISCOUS DISSIPATION EFFECTS ON STEADY MHD COMBINED HEAT AND MASS TRANSFER FLOW THROUGH A POROUS MEDIUM IN A ROTATING SYSTEM

Md. Mahmud Alam, M. Delowar Hossain[1] M. Arif Hossain[2] and Md. Ferdows[3]

Mathematics Discipline, Khulna University, Khulna-9208, Bnagladesh
[1] *Department of Mathematics, Chittagong University of Engineering & Technology, Chittagong, Bangladesh*
[2] *Department of Mathematics, Khulna University of Engineering & Technology, Khulna-9203, Bangladesh*
[3] *Department of Mathematics, Dhaka University, Dhaka-1000, Bangladesh*
e-mail: alam_mahmud2000@yahoo.com

ABSTRACT

Viscous dissipation and Joule heating effects on steady MHD combined heat and mass transfer flow through a porous medium along a semi-infinite vertical porous plate in a rotating system has been studied numerically. The boundary layer equations have been transformed into dimensionless coupled nonlinear ordinary differential equations by appropriate transformations. The similarity solutions of the transformed dimensionless equations for the flow field and heat and mass transfer characteristics are obtained by shooting iteration technique. Numerical results are presented in the form of primary and secondary velocities and temperature distributions within the boundary layer for different parameters entering into the analysis.

Keywords: *Viscous dissipation, Joule heating, rotating system, Porous plate & Porous medium*

1. INTRODUCTION

In a rotating system, the Coriolis force is very significant as compared to viscous and inertia forces occurring in the basic fluid equations. Considering this aspect of the rotational flows, model studies were carried out on MHD free convection and mass transfer flows in a rotating medium by many investigators. Considering this aspect of the rotational flows, model studies were carried out on MHD free convection and mass transfer flows in a rotating medium by many investigators of whom the names Debnath [1], Debnath *et al.*[2], Raptis and Perdikis [3] are worth mentioning.

In the above-mentioned work, the *Soret* and *Dufour* effects were neglected on the basis that they are of a smaller order of magnitude than the effects described by Fourier's and Fick's laws. However, exceptions are observed therein. The thermal diffusion (Soret) effect, for instance, has been utilized for isotope separation and in mixture between gases with very light molecular weight (H_2, H_e) and of medium molecular weight (N_2, air), the diffusion-thermo (Dufour) effect was found to be of order of considerable magnitude such that it cannot be ignored Eckert and Drake [4].

In view of the importance of above-mentioned effects, quite recently, Alam and Rahman [5] investigated the Dufour and Soret effects on mixed convection flow past a vertical porous flat plate with variable suction.

Hence, our objective is to investigate the steady MHD combined heat and mass transfer flow through a porous medium past an infinite vertical porous plate with viscous dissipation and *Joule* heating effects in a rotating system. The governing equations of the problem contain the partial differential equations, which are transformed by similarity transformation into dimensionless ordinary coupled non-linear differential equations. The obtained equations are solved numerically by sixth

order *Runge-Kutta* method along with the *Nachtsheim-Swigert* iteration technique. The obtained solutions are shown graphically.

2. THE GOVERNING EQUATIONS

A steady MHD combined heat and mass transfer flow of an electrically conducting viscous fluid through a porous medium along semi-infinite vertical porous plate $y = 0$ in a rotating system has been considered. *The flow is also assumed to be moving with a uniform velocity* U_o*, which in the* x*-direction is taken along the plate in the upward direction and* y*-axis is normal to it.* Initially the plate is at rest, after that the whole system is allowed to rotate with a constant angular velocity Ω about the y-axis. The temperature and the species concentration at the plate are constantly raised from T_w and C_w to T_∞ and C_∞ respectively, which are thereafter maintained constant, where T_∞ and C_∞ are the temperature and species concentration of the uniform flow respectively. A uniform magnetic field $\mathbf{B}$ is taken to be acting along the $y-$axis which is assumed to be electrically non-conducting. We assumed that the magnetic Reynolds number of the flow is taken to be small enough so that the induced magnetic field is negligible in comparison with applied one, so that $\mathbf{B} = (0, B_0, 0)$ and the magnetic lines of force are fixed relative to the fluid. The physical configuration considered here is shown in fig. 1. It is assumed that the plate is semi-infinite in extent and hence all the physical quantities depend on y and *x.* Thus accordance with the above assumptions and Boussinesq's approximation, the basic equations relevant to the problem are;

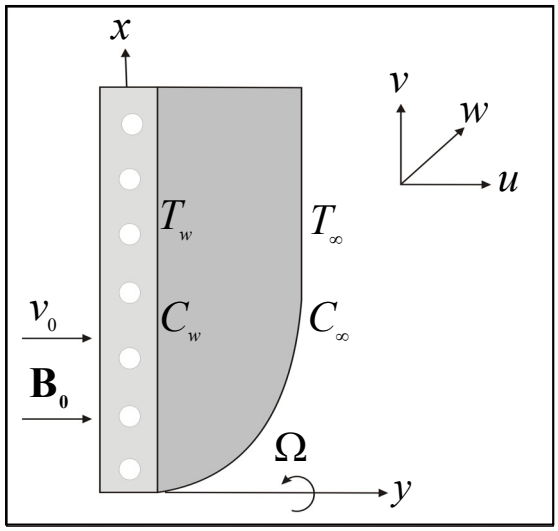

Fig. 1 Physical configuration and coordinate sysrem

$$\frac{\partial u}{\partial x} + \frac{\partial v}{\partial y} = 0 \tag{1}$$

$$u\frac{\partial u}{\partial x} + v\frac{\partial u}{\partial y} = \upsilon\frac{\partial^2 u}{\partial y^2} + g\beta\left(T - T_\infty\right) + g\beta^*\left(C - C_\infty\right) + 2\Omega w + \frac{\upsilon}{K'}\left(U_0 - u\right) + \frac{\sigma' {B_0}^2}{\rho}\left(U_0 - u\right) \tag{2}$$

$$u\frac{\partial w}{\partial x} + v\frac{\partial w}{\partial y} = \upsilon\frac{\partial^2 w}{\partial y^2} + 2\Omega\left(U_0 - u\right) - \frac{\upsilon}{K'}w - \frac{\sigma' {B_0}^2 w}{\rho} \tag{3}$$

$$u\frac{\partial T}{\partial x} + v\frac{\partial T}{\partial y} = \frac{k}{\rho c_p}\frac{\partial^2 T}{\partial y^2} + \frac{D_m k_T}{c_s c_p}\frac{\partial^2 C}{\partial y^2} + \frac{\upsilon}{c_p}\left[\left(\frac{\partial u}{\partial y}\right)^2 + \left(\frac{\partial w}{\partial y}\right)^2\right] + \frac{\sigma' B_0^2}{\rho c_p}\left[u^2 + w^2\right] \tag{4}$$

$$u\frac{\partial C}{\partial x} + v\frac{\partial C}{\partial y} = D_m\frac{\partial^2 C}{\partial y^2} + \frac{D_m k_T}{T_m}\frac{\partial^2 T}{\partial y^2} \tag{5}$$

The boundary conditions for the problem are;

$$\left.\begin{array}{ll} u = 0, v = v_0(x), & w = 0, T = T_w, \; C = C_w \quad at \; y = 0 \\ u = U_0, & w = 0, T \to T_\infty, C \to C_\infty \; as \; y \to \infty \end{array}\right\} \tag{6}$$

Following the work of Sattar [6], a transformation is now made as, $u_1 = U_0 - u \quad \therefore u = U_0 - u_1$.

In order to solve the above equations under the boundary conditions, we adopt the following similarity transformations,

$\eta = y\sqrt{\frac{U_0}{2\upsilon x}}$, $g_0(\eta) = \frac{w}{U_0}$, $\theta(\eta) = \frac{T - T_\infty}{T_w - T_\infty}$, $\phi(\eta) = \frac{C - C_\infty}{\bar{x}(C_0 - C_\infty)}$, $\psi = \sqrt{2\upsilon x U_0} f(\eta)$,

$u_1 = \frac{\partial \psi}{\partial y} = U_0 f'(\eta)$ and $\frac{u}{U_0} = 1 - f'(\eta)$, where C_0 is considered to be mean concentration and $\bar{x} = \frac{xU_0}{\upsilon}$. The continuity equation (1) then yields; $v = \frac{\partial \psi}{\partial x} = -\sqrt{\frac{\upsilon U_0}{2x}}\left[\eta f'(\eta) - f(\eta)\right]$. Also we have, $f_w = v_0(x)\sqrt{\frac{2x}{U_o \upsilon}}$, where f_w is the suction parameter or transpiration parameter and clearly, $f_w < 0$ corresponds to suction and $f_w > 0$ corresponds to injection at the plate. Now for reasons of similarity, the plate concentration is assumed to be $C_w(x) = C_\infty + \bar{x}(C_0 - C_\infty)$, where all symbols have their usual meaning.

From equations (1) - (6) and the above mentioned transformations, we have the following dimensionless ordinary coupled non-linear differential equations;

$$f''' + (\eta - 1) f'' - G_r\theta - G_m\phi - Rg_0 - (K + M) f' = 0 \tag{7}$$

$$g_0'' + (\eta - f) g_0' + Rf' - (K + M) g_0 = 0 \tag{8}$$

$$\theta'' + P_r(\eta - f)\theta' + D_f\phi'' + P_r E_c\left\{(f'')^2 + (g_0')^2\right\} + P_r E_c M\left\{(f')^2 + (g_0)^2\right\} = 0 \tag{9}$$

$$\phi'' + S_c(\eta - f)\phi' + 2S_c(f' - 1)\phi + S_0\theta'' = 0 \tag{10}$$

with the corresponding boundary conditions

$$\left.\begin{array}{l} f = f_w,\ f' = 1,\ g_0 = 0,\ \theta = 1,\ \phi = 1 \quad \text{at } \eta = 0 \\ f' = 0, \qquad g_0 = 0,\ \theta = 0,\ \phi = 0 \quad \text{as } \eta \to \infty \end{array}\right\} \tag{11}$$

where $G_r = \frac{g\beta(T_w - T_\infty)2x^3}{\upsilon^2}$ is the *Grashof* number, $G_m = \frac{g\beta^*(C_w - C_\infty)2x^3}{\upsilon^2}$ the modified *Grashof* number, $K = \frac{2\upsilon x}{K' U_0}$ the Permeability parameter, $M = \frac{2x\sigma' {B_0}^2}{\rho U_0}$ the Magnetic parameter and $R = \frac{4\Omega x}{U_0}$ the rotational parameter, $P_r = \frac{\rho \upsilon c_p}{\kappa}$ the Prandtl number, $D_f = \frac{D_m k_T \rho}{c_s K'}\frac{(C_w - C_\infty)}{(T_w - T_\infty)}$ the Dufour number, $E_c = \frac{U_0^2}{c_p(T_w - T_\infty)}$ the *Eckert* number, $S_c = \frac{\upsilon}{D_m}$ the Schmidt number and $S_0 = \frac{k_T}{T_m}\frac{(T_w - T_\infty)}{(C_w - C_\infty)}$ the Soret number.

4. SKIN-FRICTION COEFFICIENTS, NUSSELT NUMBER AND SHERWOOD NUMBER

The quantities of chief physical interest are the skin friction coefficients, the *Nusselt* number and the *Sherwood* number. The wall skin frictions are denoted by $\tau_x = \mu\left(\frac{\partial u}{\partial y}\right)_{y=0}$ and $\tau_z = \mu\left(\frac{\partial w}{\partial y}\right)_{y=0}$ which are proportional to $\left(\frac{\partial^2 f}{\partial \eta^2}\right)_{\eta=0}$ and $\left(\frac{\partial g_0}{\partial \eta}\right)_{\eta=0}$. The Nusselt number is denoted by $N_u = -\frac{1}{\Delta T}\left(\frac{\partial T}{\partial y}\right)_{y=0}$ which is proportional to $\left(\frac{\partial \theta}{\partial \eta}\right)_{\eta=0}$. The Sherwood number is denoted by $S_h = -\frac{1}{\Delta C}\left(\frac{\partial C}{\partial y}\right)_{y=0}$ which is proportional to $\left(\frac{\partial \phi}{\partial \eta}\right)_{\eta=0}$.

6. RESULTS AND DISCUSSION

The system of non-linear ordinary differential equations (7)-(10) together with the boundary conditions (11) are similar and solved numerically using Nachtsheim-Swigert shooting iteration technique (guessing the missing value) along with sixth order Runge-Kutta initial value problem solver.

It is found that the solutions are affected by the parameters, namely suction parameter f_w, Grashof number G_r, modified Grashof number G_m, Magnetic parameter M, Prandtl number P_r, *Eckert* number E_c, *Dufour* number D_f, *Schmidt* number S_c, *Soret* number S_o, Rotation parameter R. The values of G_r, G_m are taken to be large, since these values corresponds to a cooling problem, that is generally encountered in nuclear engineering in connection with the cooling of reactors.

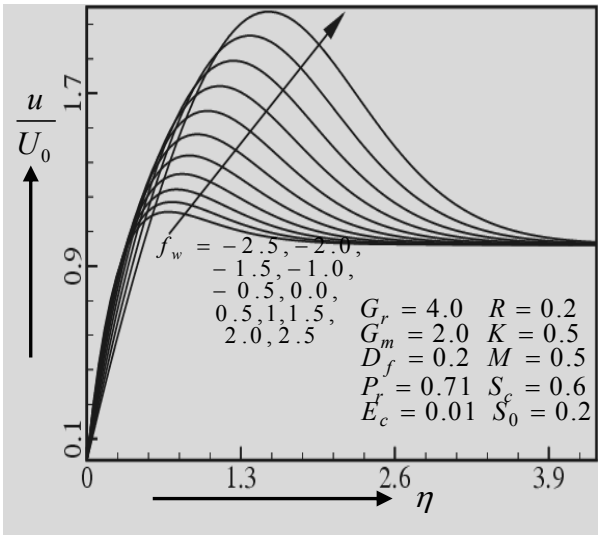

Fig. 2 Primary velocity profiles for different values of f_w

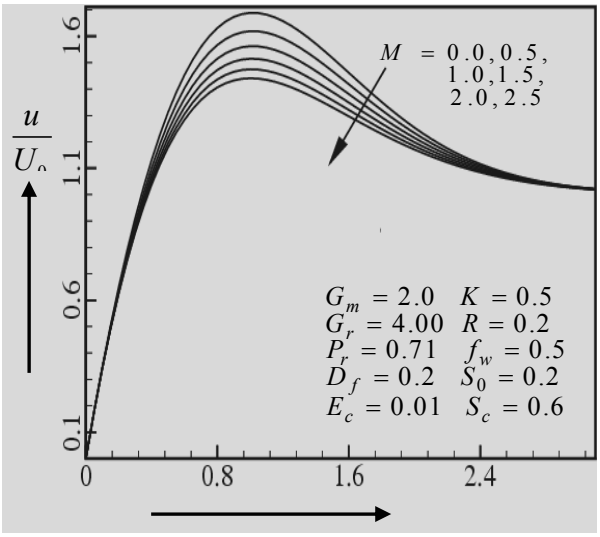

Fig. 3 Primary velocity profiles for different values of M

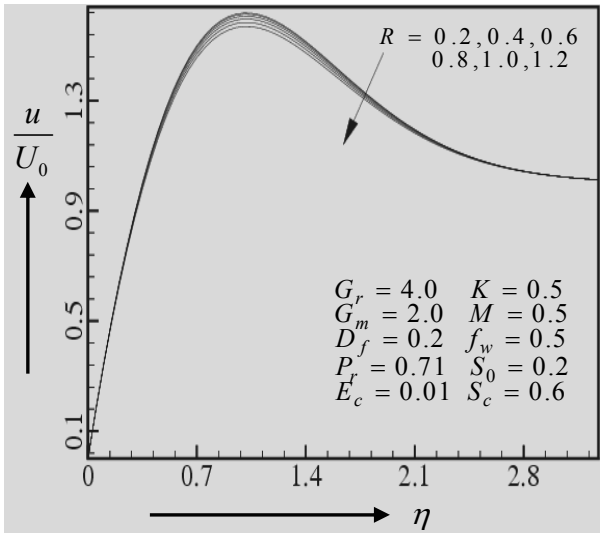

Fig. 4 Primary velocity profiles for different values of R

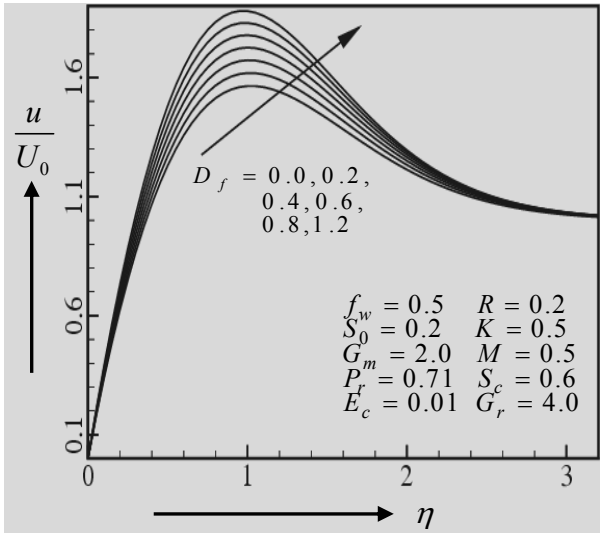

Fig. 5 Primary velocity profiles for different values of D_f

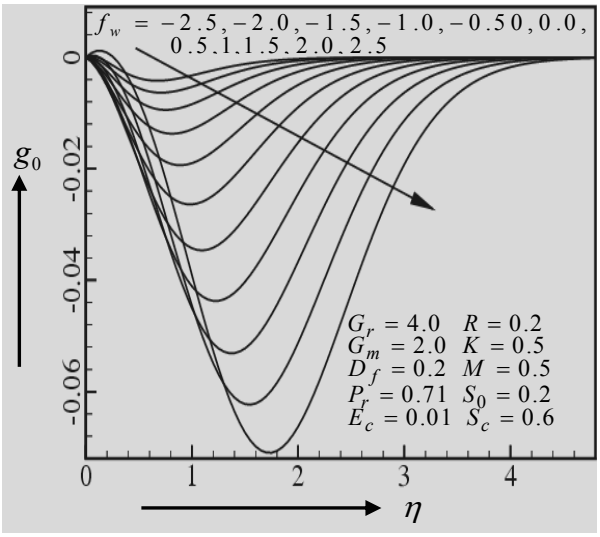

Fig. 6 Secondary velocity profiles for different values of f_w

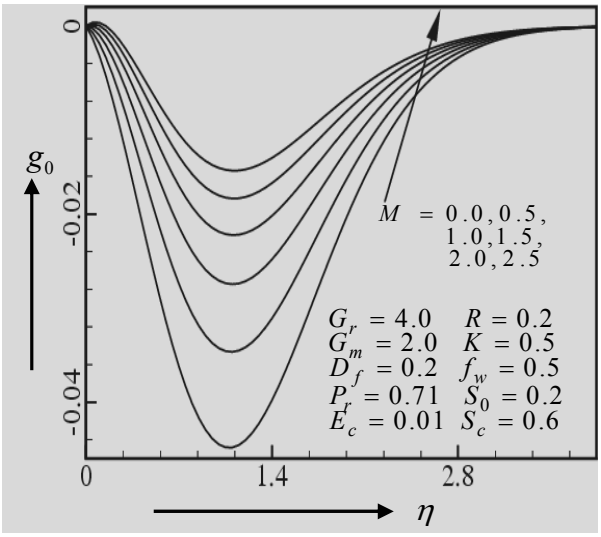

Fig. 7 Secondary velocity profiles for different values of M

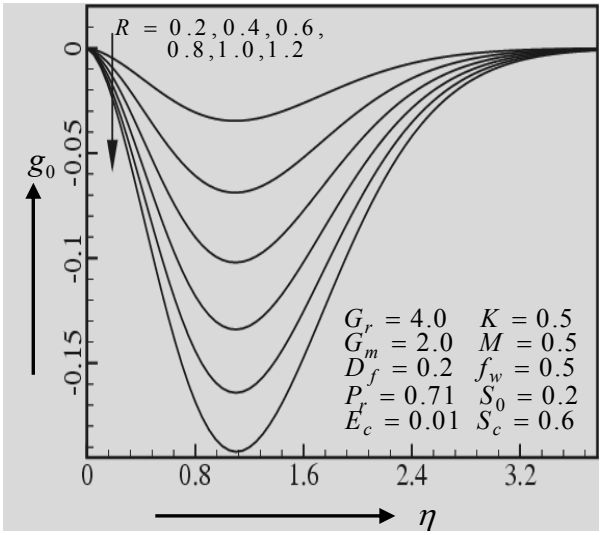

Fig. 8 Secondary velocity profiles for different values of R

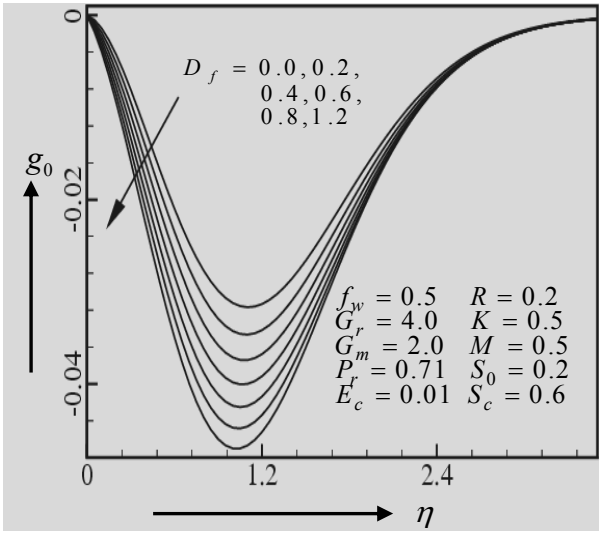

Fig. 9 Secondary velocity profiles for different values of D_f

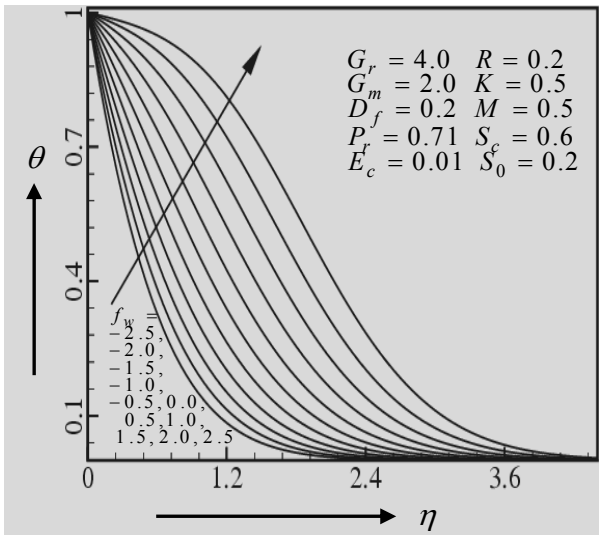

Fig. 10 Temperature profiles for different values of f_w

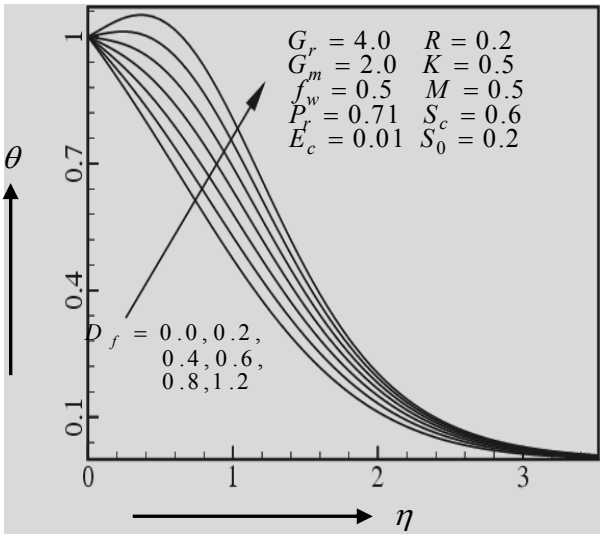

Fig. 11 Temperature profiles for different values of D_f

From fig. 2, it can be seen that the primary velocity increases with the increase of suction parameter f_w, for both $f_w > 0$ and $f_w < 0$, indicating the usual fact that suction stabilizes the boundary layer growth. fig. 3, shows the primary velocity for different values of magnetic parameter M and has a decreasing effect with increase of M. The variation of the primary velocity for different values of rotation parameter R is shown in fig. 4. It is seen that the rotation parameter R has a minor decreasing effect on the primary velocity. In fig. 5 the variations of the primary velocity for different values of Dufour number D_f shown. From this figure it is observed that the primary velocity uniformly increases with the increase of Dufour number D_f.

From fig. 6, it can be seen that the secondary velocity decreases with the increase of suction parameter f_w, for both $f_w > 0$ and $f_w < 0$, indicating the usual fact that suction stabilizes the boundary layer growth. fig. 7 shows the secondary velocity for different values of magnetic parameter M and shows a large increasing effect with the increase of M. In fig. 8 and fig. 9 the variations of the secondary velocity for different values of rotation parameter R and Dufour number D_f are shown. From these figures it is observed that the secondary velocity largely decreases with the increase of rotation parameter R and Dufour number D_f.

In fig.10, the temperature profile for different values of the suction parameter f_w is shown. It is observed from this figure that the temperature increases uniformly with the increase of suction parameter f_w. In fig.11, the temperature profile for different values of Dufour number D_f is shown. It is observed from this figure that the temperature increases as the Dufour number D_f increases.

7. REFERENCES

[1] Debnath, L. Inertial oscillations and hydromagnetic multiple boundary layers in a rotating fluid. *ZAMM,* **55**, (1975) 141.

[2] Debnath, L., Roy, S. C. and Chatterjee, A. K., Effects of hall current on unsteady hydromagnetic flow past a porous plate in a rotating fluid system. *SAMM,* **59**, (1979) 469.

[3] Raptis, A. A., Perdikis, C.P., Effects of mass transfer and free convection currents on the flow past an infinite porous plate in a rotating fluid, *Astrophysics and Space Science,* **94(2),** (1982)311.

[4] Eckert, E. R. G., Drake, R. M., Analysis of Heat and Mass Transfer, McGraw- Hill Book Co., New York (1972).

[5] Alam, M.S., Rahman, M.M., Dufour and soret effects on mixed convection flow past a vertical porous flat plate with variable suction, *Nonlinear Aanalysis: Modeling and* Control, Vol. **11**, No. 1, (2006)1-10.

[6] Sattar, M. A., Free and forced convection boundary layer flow through porous medium with large suction, *International Journal of Energy Research*, 17, (1993) p.1-7.

"Proceedings of the 4th BSME-ASME International Conference on Thermal Engineering
27-29 December, 2008, Dhaka, Bangladesh"

EFFECTS OF FORCED WAVE AND SURFACTANT ON STEAM ABSORPTION IN FALLING FILM OF AQUEOUS LiBr SOLUTION

Mohammad Ariful Islam[1], Akio Miyara[2], Toshiaki Setoguchi[2]

[1]Department of Mechanical Engineering
Khulna University of Engineering & Technology, Khulna-920300, Bangladesh, E-mail: arifbitk@yahoo.com

[2]Department of Mechanical Engineering
Saga University, 1 Honjomachi, Saga-Shi, 849-8502, Japan, Email: miyara@me.saga-u.ac.jp

ABSTRACT

Numerical simulations are performed to investigate the effects of forced wave and surfactant on steam absorption in falling film of LiBr aqueous solution. The simulation is based on a finite difference method and the governing equations are discretized on the staggered grid fixed on the physical space with constant mesh sizes. Forced waves are generated by periodically disturbed inflow boundary and result showed that forced wave produces recirculation in the solution and this recirculation moves the concentrated solution to the interface and enhance the absorption. For surfactant simulation, surface tension derivates with respect to interface temperature and concentration are given from literature and result showed that surface tension gradient produces Marangoni effect in upstream region and which lead to formation of surface waves in the downstream.

Keywords: *Steam absorption, LiBr aqueous solution, Forced wave, Surfactant, Falling film.*

1. INTRODUCTION

Absorber is the most critical component of a vapor absorption refrigeration system. Since the performance of an absorber has a significant effect on overall system performance and cost, enhancement of absorption is important. Absorption enhancement techniques can be classified into three categories: chemical treatment, nanotechnology and mechanical treatment. In the case of chemical treatment, addition of surfactant in working solution induces Marangoni convection which enhances the heat and mass transfer. Experimental and numerical studies showed that surfactant enhance the absorption rate. Kashiwagi et al. [1] and Hozawa et al. [2] explained the absorption enhancement mechanism by surfactant. In the case of mechanical treatment, heat and mass transfer can be improved by using extended surface, rotating disk, surface wave etc. Patnaik and Perez-Blanco [3] showed that surface waves can enhance the absorption rate over smooth film. Hydrodynamics of falling liquid film has a vital role in heat and mass transfer. It is well known that falling films are inherently unstable and this instability leads to formation of waves on film surface. These interfacial waves create recirculation in the film and enhance the heat and mass transfer.

In this study, effects of forced wave and surfactant on stream absorption have been investigated using numerical technique. Wave dynamics and steam absorption behavior have been analyzed.

2. COMPUTATIONAL MODEL AND NUMERICAL METHODS

A two-dimensional liquid film of aqueous LiBr solution is falling down along a vertical plane as shown in Fig. 1. Steam is being absorbed in the interface by aqueous LiBr solution. Wall is maintained at constant temperature.

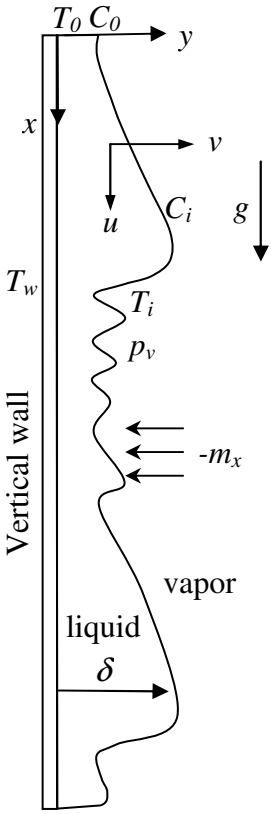

Fig.1. Physical model of the computational domain

2.1 Governing equations:

Following governing equations are solved.

Continuity equation

$$\frac{\partial u}{\partial x}+\frac{\partial v}{\partial y}=0 \tag{1}$$

Navier-Stokes equation:

$$\frac{\partial u}{\partial t}+u\frac{\partial u}{\partial x}+v\frac{\partial u}{\partial y}=-\frac{1}{\rho}\frac{\partial p}{\partial x}+\frac{\mu}{\rho}\left(\frac{\partial^2 u}{\partial x^2}+\frac{\partial^2 u}{\partial y^2}\right)+g \tag{2}$$

$$\frac{\partial v}{\partial t}+u\frac{\partial v}{\partial x}+v\frac{\partial v}{\partial y}=-\frac{1}{\rho}\frac{\partial p}{\partial y}+\frac{\mu}{\rho}\left(\frac{\partial^2 v}{\partial x^2}+\frac{\partial^2 v}{\partial y^2}\right) \tag{3}$$

Energy equation:

$$\frac{\partial T}{\partial t}+u\frac{\partial T}{\partial x}+v\frac{\partial T}{\partial y}=\alpha\left(\frac{\partial^2 T}{\partial x^2}+\frac{\partial^2 T}{\partial y^2}\right) \tag{4}$$

Mass balance equation for species, LiBr

$$\frac{\partial C}{\partial t}+u\frac{\partial C}{\partial x}+v\frac{\partial C}{\partial y}=D\left(\frac{\partial^2 C}{\partial x^2}+\frac{\partial^2 C}{\partial y^2}\right) \tag{5}$$

2.2 Boundary conditions:

At the wall surface, non-slip condition, constant temperature and non-permeable condition are assumed.

$$u=0,\ v=0,\ T=T_w,\ \frac{\partial C}{\partial y}=0 \tag{6a-d}$$

For the forced wave simulation, film thickness at inflow boundary is periodically disturbed with the following equation.

$$\delta=\delta_0+\varepsilon\sin(2\pi ft) \tag{7}$$

Where, δ_0 is the film thickness calculated from Nusselt theory. The amplitude of the disturbance wave is given as ε=0.05δ_0. The magnitude of the amplitude affects wave growth rate while effects on the fully developed waves are small. In this simulation, disturbance frequency f is given 20 Hz. For the surfactant simulation, film thickness in the inflow boundary is given by δ_0. In both cases, velocity profile in the inflow boundary is given by Nusselt velocity profile. Uniform temperature and concentration profiles are given.

Temporal film thickness variation is calculated using following kinematic boundary condition

$$\frac{\partial \delta}{\partial t}=v_i-u_i\frac{\partial \delta}{\partial x}-\frac{m_x}{\rho_l} \tag{8a}$$

Because calculated film thickness of new time step is not satisfied mass conservation due to truncation error, a correction of the new film thickness is required. An equation and procedure for the correction is presented in elsewhere [4]. Vapor pressure is assumed to be constant. Film surface pressure is calculated from normal direction force and momentum balance equation.

$$p_i=p_v-\sigma\frac{\partial^2\delta/\partial x^2}{\left[1+(\partial\delta/\partial x)^2\right]^{3/2}}+\frac{2\mu_l}{\left[1+(\partial\delta/\partial x)^2\right]}\times\left[\frac{\partial u}{\partial x}\left(\frac{\partial\delta}{\partial x}\right)^2-\left(\frac{\partial u}{\partial y}+\frac{\partial v}{\partial x}\right)\frac{\partial\delta}{\partial x}+\frac{\partial v}{\partial y}\right]_i+\frac{m_x^2}{\rho_l\left(1+(\partial\delta/\partial x)^2\right)}\left(\frac{\rho_l}{\rho_v}-1\right) \tag{8b}$$

By assuming negligible shear stress from the vapor and variable surface tension, tangential direction force and momentum balance equation becomes

$$\left(\frac{\partial u}{\partial y}+\frac{\partial v}{\partial x}\right)\left[1-\left(\frac{\partial \delta}{\partial x}\right)^2\right]-2\frac{\partial \delta}{\partial x}\left(\frac{\partial u}{\partial x}-\frac{\partial v}{\partial y}\right)=\frac{1}{\mu_l}\left(\sqrt{1+\left(\frac{\partial \delta}{\partial x}\right)^2}\right)\left(\frac{\partial \sigma}{\partial x}+\frac{\partial \delta}{\partial x}\frac{\partial \sigma}{\partial y}\right) \tag{8c}$$

Eq.(8c) is used to calculate surface velocity. Interface equilibrium concentration is a function of interface temperature and vapor pressure. It was assumed that equilibrium concentration is not affected by pressure calculated by eq. (8b). Relation between interface concentration and temperature is given by McNeely equilibrium relation [5] at vapor pressure. Surface tension is a function of interface temperature and concentration. For forced wave simulation, a simplified relation for surface tension with interface temperature and concentration is derived by fitting the experimental data of Hasaba et al. [6]. For surfactant simulation, change of surface tension can be calculated by the following equation.

$$d\sigma=\frac{\partial \sigma}{\partial T}dT_i+\frac{\partial \sigma}{\partial C}dC_i \tag{8d}$$

Surface tension derivatives $\partial\sigma/\partial T$ and $\partial\sigma/\partial C$ in the above equation are given $0.7541\text{x}10^{-3}$ N/(m K) and $-1.28\text{x}10^{-3}$ N/(m wt%) respectively from the experimental result of Kim et al. [7] considering 50 ppm of 2-Ethyl-1-hexanol is added to the solution as a surfactant. Absorption rate can be related to temperature and concentration gradients at the interface by following equations:

$$-m_x=\frac{\lambda}{H}\left(\frac{\partial T}{\partial y}-\frac{\partial T}{\partial x}\frac{\partial \delta}{\partial x}\right)_i=-\frac{D\rho_l}{C_i}\left(\frac{\partial C}{\partial y}-\frac{\partial C}{\partial x}\frac{\partial \delta}{\partial x}\right)_i \tag{8e}$$

At outflow boundary, following equations are employed for x-direction velocity u, pressure p, concentration C and temperature T.

$$\frac{\partial u}{\partial x}=0,\ \frac{\partial p}{\partial x}=0,\ \frac{\partial C}{\partial x}=0,\ \frac{\partial T}{\partial x}=0 \tag{9a-d}$$

From the equations (6a) and (9a) and the continuity equation, y-direction velocity becomes v=0.

2.3 Numerical Schemes and solution methods

The numerical simulation is based on a typical finite difference method and the basic equations are discretized on the staggered grid fixed on the physical space with constant mesh sizes. The convection terms and diffusion terms are discretized by the third-order upwind scheme and second-order central-difference scheme respectively. The algorithm of the time step is based on the HSMAC method.

3. RESULTS AND DISCUSSION

Length of the computation domain is 150 mm. The mesh sizes of the simulation are Δx=0.1 mm and Δy=0.0021675 mm. LiBr aqueous solution with concentration of 55wt% LiBr and temperature of 30^0C enters into solution domain through inflow boundary as laminar flow of Re=50. Constant vapor pressure of 1.222kPa is given and corresponding saturation temperature is 40ºC for 55wt% LiBr solution. Wall temperature is maintained at constant temperature of 30^oC. Film thickness and surface velocity at the inflow boundary are δ_0=0.43mm and u_0=0.40m/s. Simulations are performed for constant physical properties except surface tension.

Film thickness and absorption rate variations with downstream distance are shown in Fig. 2 for forced wave and surfactant simulation. For comparison, a smooth film simulation result is also included in the figure. In the case forced wave, inflow disturbance creates periodic solitary waves with capillary ripples. Instantaneous local absorption rate is higher near inflow

boundary due to cooler and stronger solution enters to the domain. Local absorption rate fluctuates with the wave profile. However, magnitude of absorption rate decreases as it moves downward. Absorption rate is higher in the wave trail and wave back and lower in the wave peak. Capillary ripples also increase the absorption rate. For surfactant simulation, small film thickness variation is appeared in upstream region though it is not visible in the in the figure. However, this small disturbance introduces surface wave in the downstream and which shows higher absorption rate than smooth film. Interface temperature and concentration of the film are shown in Fig. 3. Variations of interface temperature and concentration show similar trends as they are related with each other by a linear relation in equilibrium. In the case of smooth film, they are increased near inflow boundary and then become almost constant with downstream distance. However, in the case of forced wave they are fluctuating with wave profile. Average temperature and concentration are lower than smooth film. For the case of surfactant, interface temperature and concentration follow similar treads of smooth film in the upstream region. However, values are lower than smooth film, which clearly indicates that due to the effect of surfactant interfacial heat and mass transfer are enhanced. In the downstream region, they are fluctuated due to surface wave.

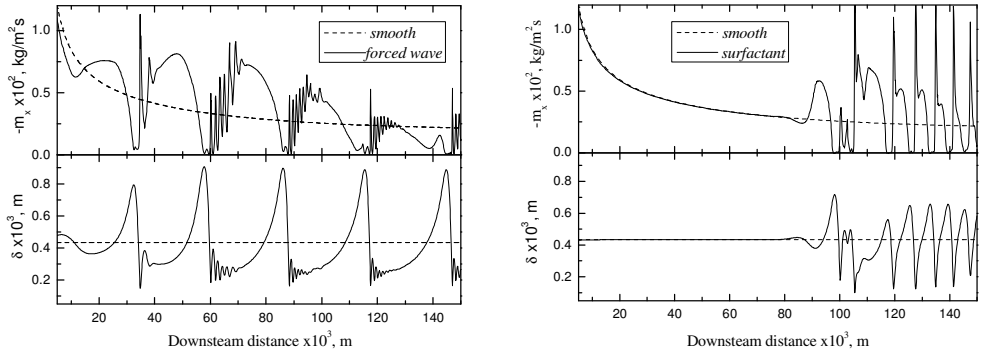

(a) **(b)**

Fig.2. Instantaneous film thickness and local absorption rate of falling film for (a) forced wave simulation (b) surfactant simulation

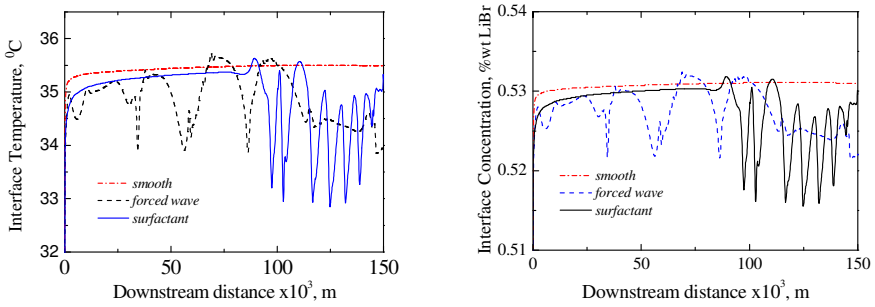

(a) **(b)**

Fig.3. Variation of (a) interface temperature (b) interface concentration

To demonstrate the insight of the film, streamlines, temperature and concentration contour of the full computational domain are shown in Fig. 4. For forced wave simulation, due inflow disturbance surface wave is appeared in the interface. Streamlines showed that surface wave produced recirculation in the wave and this recirculation moved concentrated and cooler solution to interface. For surfactant simulation, streamlines showed that in the upstream region small disturbance is appeared. However, effect of this recirculation is not significant in the temperature and concentration contour. In the downstream region, surface waves are appeared. These surface

waves produce recirculation in the film and which have significant effect on temperature and concentration field.

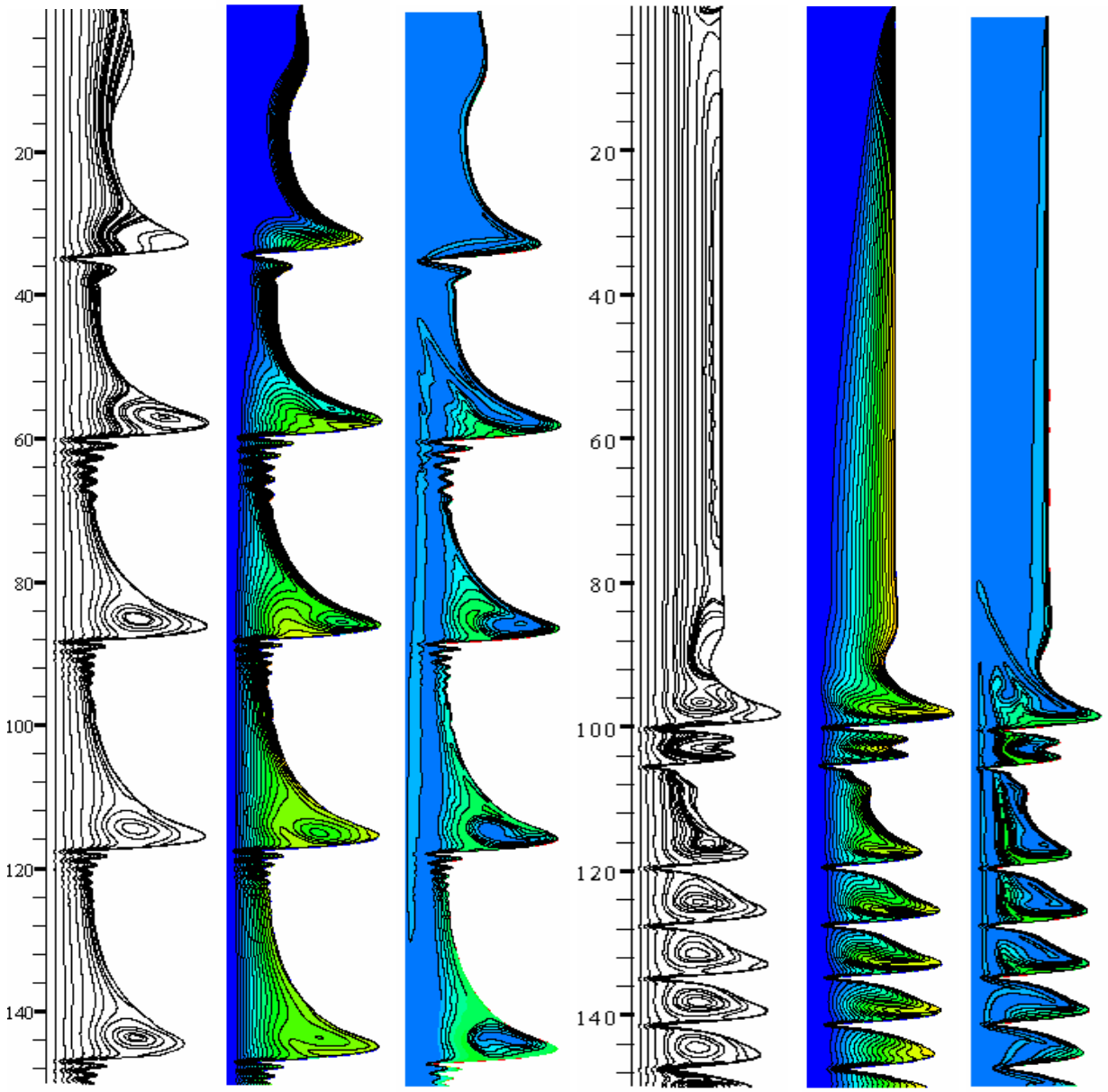

(a) (b) (c) (d) (e) (f)

Fig.4. Streamlines, temperature contour and concentration contour for forced wave simulation (a, b &c) and for surfactant simulation (d, e & f)

To compare the overall performance of forced wave, surfactant and smooth film simulations, total absorption rate is calculated using Eq. (10) and shown in Fig. 5.

$$M_x = \int_0^x m_x dx \tag{11}$$

Smooth film showed higher absorption rate near inflow boundary. However, forced wave simulation showed higher total absorption rate than smooth and surfactant simulation in the downstream. Surfactant simulation also showed higher absorption rate than smooth film in the downstream.

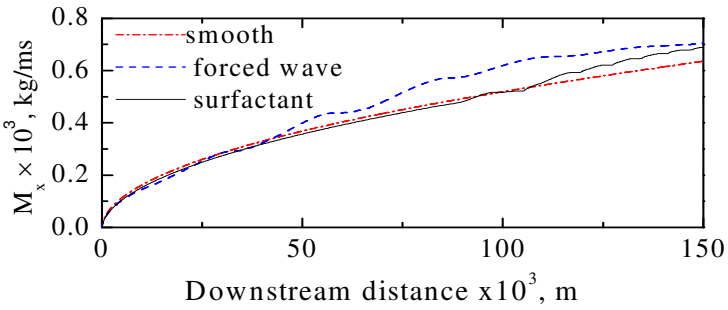

Fig.5. Total absorption rate.

4. CONCLUSIONS

A two dimensional numerical simulation of steam absorption by wavy falling LiBr aqueous solution has been performed. For forced wave simulation, waves are created by disturbing the inlet by a disturbing frequency. Result showed that wave produces recirculation in the solution and this recirculation moves the concentrated solution to the interface and enhance the absorption. For surfactant simulation, surface tension gradient produces Marangoni effects and which lead to formation of surface waves in the downstream. Total absorption rate of forced wave and surfactant simulation is higher than smooth film.

NOMENCLATURE

C	concentration of LiBr [%wt]	u	velocity in x-direction [m/s]
D	diffusion coefficient [m^2/s]	v	velocity in y-direction [m/s]
f	disturbance frequency [Hz]	α	thermal diffusivity [m^2/s]
H	heat of absorption [kJ/kg]	δ	film thickness [m]
m_x	absorption rate [kg/m^2s]	ρ	density [kg/m^3]
p	pressure [N/m^2]	λ	thermal conductivity [W/(mK)]
Re	film Reynolds number $(= \rho\bar{u}\delta_0/\mu)$	μ	viscosity [Pa.s]
T	temperature [^oC]	σ	surface tension [N/m]

REFERENCES

1. T. Kashiwagi, Y. Kurosaki, H. Shishido, Enhancement of vapor absorption into a solution using the Marangoni effect, *Trans. Jpn. Soc. Mech. Eng* 51 463, B (1985) 1002.
2. M. Hozawa, M. Ionue, J. Sato, T. Tsukada, N. Imaishi, Marangoni convection during steam absorption into aqueous LiBr solution with surfactant, *Journal of Chemical Engineering of Japan* 24(1991), 209–214.
3. V. Patnaik, H. Perez-Blanco, A study of absorption enhancement by wavy film flows, *International Journal of Heat and Fluid Flow* 17(1) (1996),71-77.
4. A. Miyara, Numerical simulation of wavy liquid film flowing down on a vertical wall and an inclined wall, *Int. J. Thermal Sci*. 39(2000), 1015 -1027.
5. L.A. McNeely, Thermodynamic properties of aqueous-solutions of lithium bromide. *ASHRAE Journal* 20(12) (1978), 54-55.
6. S. Hasaba, T. Uemura, H. Narita , Some thermal and physical properties of lithium bromide-water solutions for the designing of absorption refrigerating machines, Refrigeration 36 (405) (1959), 622-629.
7. K. J. Kim , N. S. Berman and B. D. Wood, Surface tension of aqueous Lithium Bromide + 2-Ethyl-1-hexanol, *J. Chem. Eng. Data* 39(1994), 122-124.